is that they are homogeneously dispersed in the plasma phase and therefore can deliver O_2 more homogeneously to the periphery than RBCs because microvascular hematocrit is heterogeneous particularly in pathological states. In such conditions, HbVs with a higher O_2 affinity should show a slower O_2 unloading that would be effective for oxygenating ischemic tissues.

In conclusion, HbVs provide the unique feature of allowing for the regulation of P_{50} by modulating the amount of coencapsulated PLP (33, 45). Recent studies showed the effectiveness of HBOCs with a lower P_{50} (higher O_2 affinity) as a means of implementing O_2 delivery targeted to ischemic tissue (2, 3, 41, 43). Thus this experimental method provides data useful for the design and optimization of O_2 carriers and suggests the possible utilization of HbVs for therapeutic approaches aimed at remedying ischemic conditions.

ACKNOWLEDGMENTS

The authors greatly acknowledge A. Barra and C. Walser (University of California-San Diego) for help with the animal preparations. Dr. S. Takeoka and Dr. K. Sou (Waseda University) for the preparation of the HbVs, and Dr. D. Erni (Inselspital University Hospital, Bern, Switzerland) for meaningful discussions.

GRANTS

This study was supported in part by Health Sciences Research grants (Regulatory Science, Artificial Blood Project); the Ministry of Health, Labour and Welfare, Japan (H16-IYAKU-069, 071); Japan Society for the Promotion of Science Grant-In-Aid for Scientific Research B16300162; and National Heart, Lung, and Blood Institute Bioengineering Partnership Grant R24 HL-64395 and Grants R01 HL-40696 and R01 HL-62354. H. Sakai was an overseas research fellow of the Society of Japanese Pharmacopoeia.

REFERENCES

1. **Awasthi VD, Garcia D, Klipper R, Goins BA, and Phillips WT.** Neutral and anionic liposome-encapsulated hemoglobin: effect of postinserted poly(ethylene glycol)-distearoylphosphatidylethanolamine on distribution and circulation kinetics. *J Pharmacol Exp Ther* 309: 241–248, 2004.
2. **Baines AD, Adamson G, Wojciechowski P, Pliura D, Ho P, and Kluger R.** Effect of modifying O_2 diffusivity and delivery on glomerular and tubular function in hypoxic perfused kidney. *Am J Physiol Renal Physiol* 274: F744–F752, 1998.
3. **Baines AD and Ho P.** O_2 affinity of cross-linked hemoglobins modifies O_2 metabolism in proximal tubules. *J Appl Physiol* 95: 563–570, 2003.
4. **Buehler PW and Alayash AI.** Toxicities of hemoglobin solutions: in search of in-vitro and in-vivo model systems. *Transfusion* 44: 1516–1530, 2004.
5. **Chang TMS.** *Blood Substitutes: Principles, Methods, Products, and Clinical Trials*. Basel: Karger, 1997.
6. **Cabrales P, Sakai H, Tsai AG, Tsuchida E, and Intaglietta M.** Oxygen transport by low and normal P_{50} hemoglobin vesicles in extreme hemodilution. *Am J Physiol Heart Circ Physiol* 288: H1885–H1892, 2005. First published November 24, 2004; doi:10.1152/ajpheart.01004.2004.
7. **Contaldo C, Schramm S, Wettstein R, Sakai H, Takeoka S, Tsuchida E, Leunig M, Banic A, and Erni D.** Improved oxygenation in ischemic hamster flap tissue is correlated with increasing hemodilution with Hb vesicles and their O_2 affinity. *Am J Physiol Heart Circ Physiol* 285: H1140–H1147, 2003.
8. **Djordjevich L, Mayoral J, Miller IF, and Ivankovich AD.** Cardiorespiratory effects of exchange transfusions with synthetic erythrocytes in rats. *Crit Care Med* 15: 318–323, 1987.
9. **Duling BR and Berne RM.** Longitudinal gradients in periarteriolar oxygen tension. A possible mechanism for the participation of oxygen in the local regulation of blood flow. *Circ Res* 27: 669–678, 1970.
10. **Endrich B, Asaishi K, Gotz A, and Messmer K.** Technical report: a new chamber technique for microvascular studies inunanesthetized hamsters. *Res Exp Med (Berl)* 177: 125–134, 1980.
11. **Erni D, Wettstein R, Schramm S, Sakai H, Takeoka S, Tsuchida E, Leunig M, and Banic A.** Normovolemic hemodilution with hemoglobin-vesicle solution attenuates hypoxia in ischemic hamster flap tissue. *Am J Physiol Heart Circ Physiol* 284: H1702–H1709, 2003.
12. **Goda N, Suzuki K, Naito S, Takeoka S, Tsuchida E, Ishimura Y, Tamatani T, and Suematsu M.** Distribution of heme oxygenase isoform in rat liver: topographic basis for carbon monoxide-mediated micorvascular relaxation. *J Clin Invest* 101: 604–612, 1998.
13. **Intaglietta M, Johnson PC, and Winslow RM.** Microvascular and tissue oxygen distribution. *Cardiovasc Res* 32: 632–643, 1996.
14. **Intaglietta M, Silverman NR, and Tompkins WR.** Capillary flow velocity measurements in vivo and in situ by television methods. *Microvasc Res* 10: 165–179, 1975.
15. **Intaglietta M and Tompkins WR.** Microvascular measurements by video image shearing and splitting. *Microvasc Res* 5: 309–312, 1973.
16. **Izumi Y, Sakai H, Hamada K, Takeoka S, Yamahata Y, Kato R, Nishide H, Tsuchida E, and Kobayashi K.** Physiologic responses to exchange transfusion with hemoglobin vesicles as an artificial oxygen carrier in anesthetized rats: changes in mean arterial pressure and renal cortical tissue oxygen tension. *Crit Care Med* 24: 1869–1873, 1996.
17. **Kerger H, Torres Filho IP, Rivas M, Winslow RM, and Intaglietta M.** Systemic and subcutaneous microvascular oxygen tension in conscious Syrian golden hamsters. *Am J Physiol Heart Circ Physiol* 268: H802–H810, 1995.
18. **Kyokane Norimuzu S T, Taniai H, Yamaguchi T, Takeoka S, Tsuchida E, Naito M, Nimura Y, Ishimura Y, and Suematsu M.** Carbon monoxide from heme catabolism protects against hepatobiliary dysfunction in endotoxin-treated rat liver. *Gastroenterology* 120: 1227–1240, 2001.
19. **Linberg R, Conover CD, Shum KL, and Shorr RGL.** Increased tissue oxygenation and enhanced radiation sensitivity of solid tumors in rodents following polyethylene glycol conjugated bovine hemoglobin administration. In Vivo 12: 167–174, 1998.
20. **Lipowsky HH and Zweifach B.** Application of the "two slit" photometric technique to the measurement of microvascular volumetric flow rates. *Microvasc Res* 15: 93–101, 1978.
21. **McCarthy MR, Vandegeriff KD, and Winslow RM.** The role of facilitated diffusion in oxygen transport by cell-free hemoglobins: implications for the design of hemoglobin-based oxygen carriers. *Biophys Chem* 92: 103–117, 2001.
22. **Papenfuss HD, Gross JF, Intaglietta M, and Treese FA.** A transparent access chamber for the rat dorsal skin fold. *Microvasc Res* 18: 311–318, 1979.
23. **Richmond KN, Shonat RD, Lynch RM, and Johnson PC.** Critical P_{O_2} of skeletal muscle in vivo. *Am J Physiol Heart Circ Physiol* 277: H1831–H1840, 1999.
24. **Rudolph AS, Klipper RW, Goins B, and Phillips WT.** In vivo biodistribution of a radiolabelled blood substitute: ^{99m}Tc-labeled liposome-encapsulated hemoglobin in an anesthetized rabbit. *Proc Natl Acad Sci USA* 88: 10976–10980, 1991.
25. **Sakai H, Hara H, Tsai AG, Tsuchida E, Johnson PC, and Intaglietta M.** Changes in resistance vessels during hemorrhagic shock and resuscitation in conscious hamster model. *Am J Physiol Heart Circ Physiol* 276: H563–H571, 1999.
26. **Sakai H, Hara H, Yuasa M, Tsai AG, Takeoka S, Tsuchida E, and Intaglietta M.** Molecular dimensions of Hb-based O_2 carriers determine constriction of resistance arteries and hypertension in conscious hamster model. *Am J Physiol Heart Circ Physiol* 279: H908–H915, 2000.
27. **Sakai H, Hisamoto S, Fukutomi I, Sou K, Takeoka S, and Tsuchida E.** Detection of lipopolysaccharide in hemoglobin-vesicles by *Limulus amebocyte* lysate test with kinetic-turbidimetric gell clotting analysis and pretreatment with a surfactant. *J Pharm Sci* 93: 310–321, 2004.
28. **Sakai H, Horinouchi H, Tomiyama K, Ikeda E, Takeoka S, Kobayashi K, and Tsuchida E.** Hemoglobin-vesicles as oxygen carriers: influence on phagocytic activity and histopathological changes in reticuloendothelial systems. *Am J Pathol* 159: 1079–1088, 2001.
29. **Sakai H, Masada Y, Horinouchi H, Ikeda E, Sou K, Takeoka S, Suematsu M, Kobayashi K, and Tsuchida E.** Physiologic capacity of reticuloendothelial system for degradation of hemoglobin-vesicles (artificial oxygen carriers) after massive intravenous doses by daily repeated infusion for 14 days. *J Pharmacol Exp Ther* 311: 874–884, 2004.
30. **Sakai H, Masada Y, Horinouchi H, Yamamoto M, Ikeda E, Takeoka S, Kobayashi K, and Tsuchida E.** Hemoglobin-vesicles suspended in recombinant human serum albumin for resuscitation from hemorrhagic shock in anesthetized rats. *Crit Care Med* 32: 539–545, 2004.

31. **Sakai H, Suzuki Y, Kinoshita M, Takeoka S, Maeda N, and Tsuchida E.** O_2-release from Hb-vesicles evaluated using an artificial narrow O_2-permeable tube: comparison with RBC and acellular Hb. *Am J Physiol Heart Circ Physiol* 285: H2543–H2551, 2003.
32. **Sakai H, Takeoka S, Yokohama H, Seino Y, Nishide H, and Tsuchida E.** Purification of concentrated Hb using organic solvent and heat treatment. *Protein Expr Purif* 4: 563–569, 1993.
33. **Sakai H, Tsai AG, Rohlfs RJ, Hara H, Takeoka S, Tsuchida E, and Intaglietta M.** Microvascular responses to hemodilution with Hb-vesicles as red blood cell substitutes: influences of O_2 affinity. *Am J Physiol Heart Circ Physiol* 276: H553–H562, 1999.
34. **Sakai H, Yuasa M, Onuma H, Takeoka S, and Tsuchida E.** Synthesis and physicochemical characterization of a series of hemoglobin-based oxygen carriers: objective comparison between cellular and acellular types. *Bioconjug Chem* 11: 56–64, 2000.
35. **Shibata M, Ichioka S, Ando J, and Kamiya A.** Microvascular and interstitial P_{O_2} measurements in rat skeletal muscle by phosphorescence quenching. *J Appl Physiol* 91: 321–327, 2001.
36. **Shirasawa T, Izumizaki M, Suzuki YI, Ishihara A, Shimizu T, Tamaki M, Huang F, Koizumi KI, Iwase M, Sakai H, Tsuchida E, Ueshima U, Inoue H, Koseki H, Senda H, Kuriyama T, and Homma I.** Oxygen affinity of hemoglobin regulates O_2 consumption, metabolism, and physical activity. *J Biol Chem* 278: 5035–5043, 2003.
37. **Sou K, Naito Y, Endo T, Takeoka S, and Tsuchida E.** Effective encapsulation of proteins into size-controlled phospholipid vesicles using freeze-thawing and extrusion. *Biotechnol Progr* 19: 1547–1552, 2003.
38. **Takeoka S, Teramura Y, Atoji T, and Tsuchida E.** Effect of Hb-encapsulation with vesicles on H_2O_2 reaction and lipid peroxidation. *Bioconjug Chem* 13: 1302–1308, 2002.
39. **Tomson FN and Wardrop KJ.** Clinical chemistry and hematology. In: *Laboratory Hamsters*, edited by van Hoosier GL Jr and McPherson CW. Orlando, FL: Academic, 1987, chapt. 3, p. 43–59.
40. **Torres Filho IP and Intaglietta M.** Microvascular P_{O_2} measurements by phosphorescence decay method. *Am J Physiol Heart Circ Physiol* 265: H1434–H1438, 1993.
41. **Tsai AG, Kerger H, and Intaglietta M.** Microcirculatory consequences of blood substitutution with αα-hemoglobin. In: *Blood Substitutes: Physiological Basis of Efficacy*, edited by Winslow RM, Vandegriff K, and Intaglietta M. Boston, MA: Birkhauser, 1995, p. 155–174.
42. **Tsai AG, Friesenecker B, Mazzoni MC, Kerger H, Buerk DG, Johnson PC, and Intaglietta M.** Microvascular and tissue oxygen gradients in the rat mesentery. *Proc Natl Acad Sci USA* 95: 6590–6595, 1998.
43. **Tsai AG, Vandegriff KD, Intaglietta M, and Winslow RM.** Targeted O_2 delivery by low-P_{50} hemoglobin: a new basis for O_2 therapeutics. *Am J Physiol Heart Circ Physiol* 285: H1411–H1419, 2003.
44. **Vanderkooi JM, Maniara G, Green TJ, and Wilson DF.** An optical method for measurement of dioxygen concentration based on quenching of phosphorescence. *J Biol Chem* 262: 5476–5482, 1987.
45. **Wang L, Morizawa K, Tokuyama S, Satoh T, and Tsuchida E.** Modulation of oxygen-carrying capacity of artificial red cells (ARC). *Polymer Adv Technol* 4: 8–11, 1992.

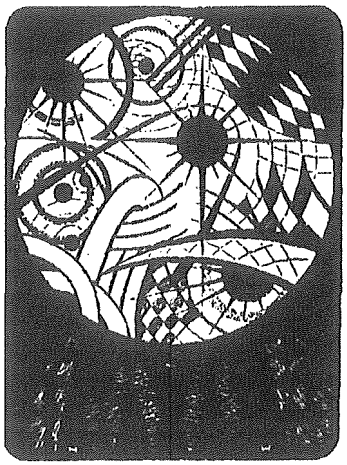

Am J Physiol Heart Circ Physiol 289: H2624–H2631, 2005.
First published August 5, 2005; doi:10.1152/ajpheart.00308.2005.

Is hemoglobin in hemoglobin vesicles infused for isovolemic hemodilution necessary to improve oxygenation in critically ischemic hamster skin?

Jan A. Plock,[1] Claudio Contaldo,[1] Hiromi Sakai,[2] Eishun Tsuchida,[2] Michael Leunig,[1] Andrej Banic,[1] Michael D. Menger,[3] and Dominique Erni[1]

[1]*Department of Orthopedic, Plastic and Hand Surgery, Inselspital University Hospital, Berne, Switzerland;*
[2]*Advanced Research Institute for Science and Engineering, Waseda University, Tokyo, Japan; and*
[3]*Institute for Clinical and Experimental Surgery, University of Saarland, Homburg/Saar, Germany*

Submitted 30 March 2005; accepted in final form 31 July 2005

Plock, Jan A., Claudio Contaldo, Hiromi Sakai, Eishun Tsuchida, Michael Leunig, Andrej Banic, Michael D. Menger, and Dominique Erni. Is hemoglobin in hemoglobin vesicles infused for isovolemic hemodilution necessary to improve oxygenation in critically ischemic hamster skin? *Am J Physiol Heart Circ Physiol* 289: H2624–H2631, 2005. First published August 5, 2005; doi:10.1152/ajpheart.00308.2005.—The aim of this study was to test the influence of hemoglobin, encapsulated in phospholipid vesicles as an oxygen carrier, given in the course of isovolemic hemodilution to improve oxygenation in critically ischemic hamster flap tissue. Capillary hemodynamics and macromolecular leakage were investigated with intravital microscopy and analyzed off-line with the CapImage software. Partial tissue oxygen tension was measured with fluorescence quenching electrodes. The occurrence of apoptosis was assessed with the terminal deoxynucleotidyl transferase-mediated dUTP nick-end labeling assay. Vesicles with (HbV) or without (V) encapsulated Hb were suspended in 6% hydroxyethyl starch (HES) used for the 33% blood exchange. In the ischemic tissue, hemodilution led to an increase in functional capillary density by 31% for HES ($P < 0.01$ vs. other groups), 66% for V-HES, and 62% for HbV-HES (all $P < 0.01$ vs. control). Capillary diameters behaved inversely proportional to capillary microhemodynamics. The 20% increase in macromolecular leakage found over time in control animals was completely abolished in the vesicles groups ($P < 0.01$) but not with HES. Oxygen tension was improved from 10.7 to 16.0 mmHg after HbV-HES ($P < 0.01$ vs. baseline and other groups). Compared with the other groups, apoptosis was significantly reduced after HbV-HES ($P < 0.01$). We conclude that the encapsulation of Hb was essential to attenuate hypoxia and subsequent cell death in the critically ischemic tissue. However, the effect was partly attributed to the rheological changes exerted by the vesicles.

blood substitutes; capillary hemodynamics; hypoxia; capillary leakage; apoptosis

CRITICAL ISCHEMIA is characterized by a reduction of nutrient blood flow, thus causing hypoxia that may eventually lead to apoptosis and cell death. One of the most frequent etiologies of critical ischemia is the acute peripheral arterial obstruction. Oxygenation and survival of ischemic myocardial (13, 24), cerebral (23, 32), and peripheral (6) tissues could successfully be improved after the infusion of solutions containing artificial oxygen carriers, such as perfluorocarbons and chemically modified Hbs.

In recent studies (8, 12), we were able to demonstrate that hypoxia in ischemic hamster flap tissue was attenuated by isovolemic hemodilution with colloid solutions supplemented with phospholipid vesicles containing isolated, purified human Hb. The effect was ascribed to the combination of an improvement of the impaired microcirculation and the presence of the Hb vesicles (HbVs) (12), and it correlated with the degree of blood exchange (8). However, it was not possible to outline the extent to which either the rheological changes or the presence of Hb contributed to this benefit. In other words, it could not be excluded that similar success could have been achieved with the use of phospholipid vesicles void of oxygen carriers, which in turn would have a significant impact on their clinical application, because the manufacturing of the vesicles could be simplified and possible adverse effects related to the encapsulated Hb could be avoided. Furthermore, it may be postulated that the presence of cell-free Hbs may lead to arteriolar vasoconstriction with (4, 26) or without (14) scavenging of nitric oxide, which may further deteriorate microvascular perfusion and oxygen delivery in the ischemic tissue.

In this context, the viscosity of the diluent appears to play a pivotal role. Because of the large size of the vesicles, the viscosity of HbV solutions is manyfold higher than that of hamster plasma (12, 26). Raising the viscosity in the plasma phase of the circulating blood led to shear stress-induced, nitric oxide-mediated arteriolar vasodilation (2, 9), which was made responsible for increasing microcirculatory blood flow (2), microvascular pressure (3), and functional capillary density (FCD) (2, 3) in healthy tissue in hamsters. Furthermore, according to the Stokes-Einstein equation, the diffusivity of oxygen through the plasma is inversely proportional to its viscosity, an effect that may contribute to the distribution of oxygen release in favor of hypoxic tissues, in which oxygen diffusion is ensured by the high gradient of partial oxygen tension.

The hypothesis to be tested in this study was whether the presence of Hb in the HbV is needed to obtain the previously reported benefit of isovolemic hemodilution with HbV on the oxygenation of the ischemic hamster flap tissue (8, 12) or whether similar effects could be obtained with a suspension of vesicles void of Hb due to their viscosity-related effect on arteriolar and capillary hemodynamics and on tissue oxygenation.

MATERIALS AND METHODS

Experiments were performed according to the National Institutes of Health guidelines for the care and use of laboratory animals and with

Address for reprint requests and other correspondence: D. Erni, Division of Plastic and Reconstructive Surgery, Inselspital Univ. Hospital, CH-3010 Berne, Switzerland (e-mail: dominique.erni@insel.ch).

The costs of publication of this article were defrayed in part by the payment of page charges. The article must therefore be hereby marked "*advertisement*" in accordance with 18 U.S.C. Section 1734 solely to indicate this fact.

the approval of the local Animal Ethics Committee. Forty-eight male Syrian golden hamsters weighing 65–85 g were used in this study. The animals were randomly assigned to the control group or to one of three groups subjected to normovolemic hemodilution with 6% hydroxyethyl starch 200–0.5 (HES; Fresenius, Stans, Switzerland) or vesicles with or without encapsulated Hb suspended in hydroxyethyl starch (HbV-HES and V-HES, respectively).

Animal and flap preparation. A hamster skin flap model was used as previously described in detail (7, 8, 10–12). Anesthesia was induced by pentobarbital sodium (Nembutal) injected intraperitoneally (100 mg/kg body wt; Abbott Laboratories, Chicago, IL). The carotid artery and external jugular vein were cannulated for administration of anesthesia, blood exchange, laboratory analysis, and monitoring arterial blood pressure (Type514; Spacelabs, Hillsboro, OR). Catheterization and flap dissection were performed with the aid of an operating microscope at ×10 magnification (Wild; Heerbrugg, Switzerland). An island flap measuring 3 × 2 cm was dissected from the shaved and epilated back skin of the animal. The flap consisted of skin and a thin layer of panniculus carnosus muscle, and it was perfused by one vascular axis, which bifurcates into two equal-sized branches within the flap, each of them supplying a separate vascular territory. One of the branches was transected after being secured with microsurgical ligatures, thus rendering the corresponding vascular territory ischemic. This tissue was merely perfused by a collateral vasculature connecting the two vascular networks. During surgery, the flap was irrigated with 0.9% NaCl solution to prevent the flap from drying out. The animal was placed on a specially designed Plexiglas stage including a platform for fixation of the flap. During surgery, 4 mg papaverine hydrochloride (Sigma Chemical, St. Louis, MO) dissolved in 1 ml physiological saline solution were applied to the pedicle by a soaked cotton tip to prevent vascular spasm.

Vesicle solutions. The vesicles were prepared as previously reported (27, 28). They consisted of a phospholipid bilayer membrane coated with polyethylene glycol encapsulating either physiological saline solution (V) or isolated and purified human hemoglobin (HbV). The sizes of V and HbV were 274 ± 32 and 253 ± 63 nm, respectively. The Hb concentration inside the HbV was ~35 g/dl, and its P_{50} was 9 mmHg, which was calculated from the O_2 equilibrium curve measured with a Hemox Analyzer (TCS Medical Products) at 37°C (33). The vesicles were suspended in a solution with a final HES concentration of 6%.

Laboratory analysis. Blood samples were collected in 40-μl heparin-washed microtubes for measurement of total Hb concentration and arterial blood gases with the use of the Radiometer ABL 625 system (Radiometer; Copenhagen, Denmark). By validating this system, we have found that the vesicle-bound hemoglobin concentration may be overestimated by maximally 10%, whereas the results were not affected by the lipid concentrations present in our study. Hematocrit was determined by centrifugation. The colloid osmotic pressure of the diluents was measured with a colloid osmometer (model 4420; Wescor, Logan, UT) with a 30-kDa cutoff membrane. The viscosity was measured with a cone-plate viscometer (PVII+; Brookfield Engineering, Middleboro, MA) or a capillary rheometer (Anton Parr DCS 300; Parr Physica, Graz, Austria) at 37°C. Viscosities of blood and plasma were measured 4 h after hemodilution with a Höppler-type viscosimeter (HAAKE Messtechnik, Karlsruhe, Germany). The physicochemical characteristics of the solutions are summarized in Table 1. Oxygen content (ml/dl) in the carotid artery was calculated according to the equation

$$[O_2] = 1.34 \cdot \{([Hb_{RBC}] \cdot So_{2RBC}) + ([Hb_{HbV}] \cdot So_{2HbV})\}, \quad (1)$$

where 1.34 corresponds to the amount of oxygen (given in milliliters) bound to 1 g of Hb at 100% saturation. So_2 is the fractional oxygen saturation of red blood cells (RBCs) and HbV, which was derived from Po_2 by using the oxygen dissociation curves of the two hemoglobins (29).

Microhemodynamic measurements. Investigations were performed with the use of an intravital microscope (Axioplan 1; Zeiss, Jena, Germany). Microscopic images were captured by a television camera (intensified charge-coupled device camera; Kappa Messtechnik, Gleichen, Germany), recorded on video (50 Hz; Panasonic, Osaka, Japan), and displayed on a television screen for subsequent off-line analysis (Trinitron PVM-1454QM; Sony, Tokyo, Japan). The preparation was observed visually with a ×40 objective with a numerical aperture of 0.75, which resulted in a theoretical resolution of ~300 nm and a total optical magnification of ×909 on the video monitor, where 1 pixel corresponded to 264 nm in the tissue. The microvessels were classified according to physiological and anatomical features into conduit arterioles (connections to each other), end arterioles, and small venules (10, 12). The vessels were chosen for examination according to their optical clarity. The intraluminal microvascular diameters were measured visually on the television screen with the use of 2% fluorescein isothiocyanate-labeled dextran (FITC dextran, molecular mass 150 kDa; Sigma Chemical, Buchs, Switzerland) injected intra-arterially (0.05 ml), an excitation filter (485–505 nm), a dichroic mirror (510 nm), and a barrier filter (530 nm). The capillary hemodynamics and macromolecular leakage were assessed with a computer-assisted image analysis system (CapImage; Zeintl Software, Heidelberg, Germany) (17). Capillary diameters were obtained from the averages of five consecutive measurements. Because the capillary diameters measured with the present technique may possibly be underestimated because of the use of fluorescence microscopy and the optical properties of the microscope (22), the values were given in percentages of the mean obtained in the anatomically perfused tissue of the control group at baseline. FCD was defined as the length of RBC-perfused capillaries per observation field and expressed in centimeters per square centimeters. The product of RBC velocity and FCD was taken as an index reflecting the perfusion of the tissue with RBCs. The endothelial integrity was assessed by measuring macromolecular leakage (18). This was achieved by densitometric analysis of the fluorescence of FITC dextran 10 min after its injection. Macromolecular leakage was expressed by the ratio of fluorescence obtained in the interstitial space versus capillary fluorescence.

Table 1. *Physicochemical characteristics of hamster blood and diluents*

	Hamster Blood	Hamster Plasma	HES	V-HES	HbV-HES
[Hb], g/dl	18	0	0	0	7.5
[metHb], %					<3
[Lipid], g/dl				4.4	4.2
Oncotic pressure, mmHg		18	36	36	36
Viscosity of solution, cP	4.5	1.2	1.9	11.5	11.5
Plasma viscosity 4 h after exchange transfusion, cP		1.34 ± 0.03	1.31 ± 0.06	1.74 ± 0.13*	1.67 ± 0.12*

Values are means ± SD. HES, 6% hydroxyethyl starch; V-HES and HbV-HES, vesicles with and without hemoglobin suspended in HES, respectively; [Hb], hemoglobin concentration; [metHb], methemoglobin concentration. [Hb] was measured by a cyanomethemoglobin method, and [lipid] was measured with enzymatic method with use of phospholipase D. Viscosity of solutions was measured at 37°C and at 150 s^{-1}; plasma viscosity was measured at 25°C. *$P <$ 0.01 vs. hamster plasma and HES.

Tissue oxygen tension. Partial tissue oxygen tension was assessed with combined bare fiber probes with a tip diameter of 450 μm (Oxylite probes; Oxford Optronix, Oxford, UK). The sensitive tip of the oxygen probe (100-μm diameter) consists of ruthenium-III-(Tris)-chloride, which measures Po_2 by fluorescence quenching of the dye. A T-type thermocouple was attached to the probe, which was coated with a biocompatible sleeve of polyurethane. According to the manufacturer, the bare fiber probe provides resolutions of <1 mmHg and 0.1°C for partial oxygen tension and temperature, respectively, and the sampling area of the oxygen sensors is 0.25–0.35 mm^3. The probes were inserted into the subcutaneous tissue in the middle of each vascular territory under visual microscopic control. Care was taken to place the probes in such a way that no arterioles or large venules lay within the sampling area.

Tissue viability. The occurrence of apoptosis was assessed with the transferase-mediated dUTP nick end-labeling (TUNEL) assay (In Situ Cell Death Detection Kit, tetramethylrhodamine red; Roche Diagnostics, Rotkreuz, Switzerland) (1). All steps were performed according to the supplier's instructions. Tissue samples were obtained from the middle of each vascular territory. The samples were transferred to gelatinized microslides and air-dried overnight at 37°C. The sections were dewaxed in xylene (three changes), rehydrated in ethanol, and rinsed in Tris-buffered saline [50 mM Tris·NaCl, pH 7.4, containing 100 mM sodium chloride (two changes)], and then incubated in 20 μg/ml proteinase K for 15 min at room temperature. Endogenous peroxidase activity was suppressed by treatment with 0.3% hydrogen peroxide for 10 min. The sections were then incubated with terminal deoxynucleotidyl transferase enzyme for 1 h at 37°C followed by peroxidase-conjugated anti-digoxigenin antibody for 30 min at room temperature. The reaction was visualized by diaminobenzidine substrate for 8 min at room temperature. Thereafter, the sections were washed three times with Tris-buffered saline. The labeled DNA fragments were visualized by incubating the sections with tetramethylrhodamine used as a fluorescence marker, and the sections were examined with a fluorescence microscope (Leica DM/RB; Leica Microsystems, Wetzlar, Germany). Data were given as the averages of fluorescent cells counted in five randomly selected visual fields (0.5 × 0.5 mm) for the dermis and epidermis separately. Sebaceous glands and hair follicles were identified and excluded from the cell counts because of their consistently high apoptosis rate.

Protocol. The animals were kept under light anesthesia with a continuous infusion of 50 mg/ml pentobarbital sodium given at a rate of ~0.5 $mg \cdot min^{-1} \cdot kg$ body wt^{-1} throughout the experiment. The depth of anesthesia was regulated by tolerance of a noxious reflex due to pinching of the hind paw but no nonaversive reflexes (palpebral, corneal, and jaw reflex) (10). A constant temperature in the animal and flap preparation was maintained by means of a heating pad and by keeping room temperature at 28°C.

Baseline values were obtained after a postoperative period of 1 h had elapsed for stabilization. Thereafter, one-third of the total blood volume was exchanged with HES or the vesicle solutions. This was achieved by simultaneous blood withdrawal via the carotid catheter and infusion via the jugular catheter over 15 min. Measurements were taken hourly until 4 h after hemodilution, and tissue samples for immunohistochemical analysis were taken after 5 h.

Exclusion criteria were abnormalities of the vascular anatomy, insufficient optical clarity, mean arterial pressure <60 mmHg, and systemic arterial pH, Po_2, and Pco_2 outside the normal ranges at baseline (7.19–7.29, 35–55, and 45–65 mmHg, respectively).

The animals were euthanized with an overdose of pentobarbital sodium at the end of the experiment.

Statistical analysis. The InStat version 3 program (Graph Pad Software; San Diego, CA) was utilized for statistical analysis. The data were presented as means ± SD. The time-related differences between repeat measurements were assessed by the paired ANOVA, followed by Dunnett's posttest. The differences between groups were assessed by the unpaired ANOVA, followed by Tukey's posttest. If only two sets of data were to be compared, paired (repeat measurements) and unpaired (differences between groups) *t*-tests were used. A value of $P < 0.05$ was taken to represent statistical significance.

RESULTS

Six animals did not fulfill the inclusion criteria and were excluded from this study, thus resulting in sample sizes of $n = 11$ for control, $n = 11$ for HES, $n = 9$ for V-HES, and $n = 11$ for HbV-HES.

The systemic data are summarized in Table 2. Similar hematocrits were obtained in all hemodiluted animals. The blood exchange reduced mean total Hb concentration to 10.4 and 10.1 g/dl for HES and V-HES, respectively, but only to 13.0 g/dl if HbV was added ($P < 0.01$ vs. other groups). Hemodilution increased arterial Po_2 to mean values of 58–61 mmHg ($P < 0.01$ vs. baseline) and decreased Pco_2 to 40–41 mmHg ($P < 0.05$), whereas pH remained virtually unchanged. Compared with the control animals, plasma viscosity was increased from 1.34 to ~1.7 cP after hemodilution with both vesicle solutions ($P < 0.01$ vs. control) but not with HES (Table 1).

Hemodilution resulted in an arterial oxygen content decrease from ~18 to 12.8 ± 1.5 ml/dl for HES and 12.6 ± 1.3 ml/dl for V-HES (both $P < 0.01$) after 4 h, whereas this reduction of oxygen-carrying capacity was significantly attenuated by adding HbV to the diluent (15.7 ± 1.2 ml/dl; $P < 0.01$ vs. baseline and other groups) (Fig. 1).

Table 2. *Systemic and laboratory data at baseline and 1 and 4 h after blood exchange*

	Baseline	1 h	4 h
MAP, mmHg			
Control	109±5	104±8	101±7
HES	105±8	107±5	99±2
V-HES	107±5	109±5	102±6
HbV-HES	105±5	107±5	103±3
Hematocrit			
Control	0.55±0.03	0.55±0.03	0.53±0.03
HES	0.57±0.03	0.33±0.03[b,d]	0.33±0.03[b,d]
V-HES	0.57±0.02	0.32±0.02[b,d]	0.32±0.01[b,d]
HbV-HES	0.56±0.02	0.33±0.02[b,d]	0.33±0.02[b,d]
Total Hb concentration, g/dl			
Control	18.0±1.1	18.0±1.4	17.2±1.1
HES	17.7±1.2	10.4±0.8[b,d]	11.2±0.8[b,d]
V-HES	17.8±1.3	10.1±0.3[b,d]	10.7±0.5[b,d]
HbV-HES	17.9±0.9	13.0±0.4[b,e]	13.2±0.7[b,e]
Po_2, mmHg			
Control	43±3	44±6	49±8
HES	42±5	52±9[a]	59±12[b]
V-HES	40±8	52±8[a]	61±15[b]
HbV-HES	44±6	57±8[b,c]	58±10[b]
Pco_2, mmHg			
Control	53±6	52±3	48±6
HES	52±4	48±5	41±7[a]
V-HES	51±6	43±8[a,c]	40±11[a]
HbV-HES	51±7	43±8[a,c]	41±6[a]
pH			
Control	7.34±0.04	7.34±0.05	7.36±0.05
HES	7.35±0.05	7.39±0.05	7.39±0.07
V-HES	7.33±0.05	7.38±0.06	7.37±0.08
HbV-HES	7.34±0.06	7.37±0.06	7.34±0.04

Values are means ± SD. MAP, mean arterial pressure. [a]$P < 0.05$ and [b]$P < 0.01$ vs. baseline; [c]$P < 0.05$ and [d]$P < 0.01$ vs. control; [e]$P < 0.01$ vs. other groups.

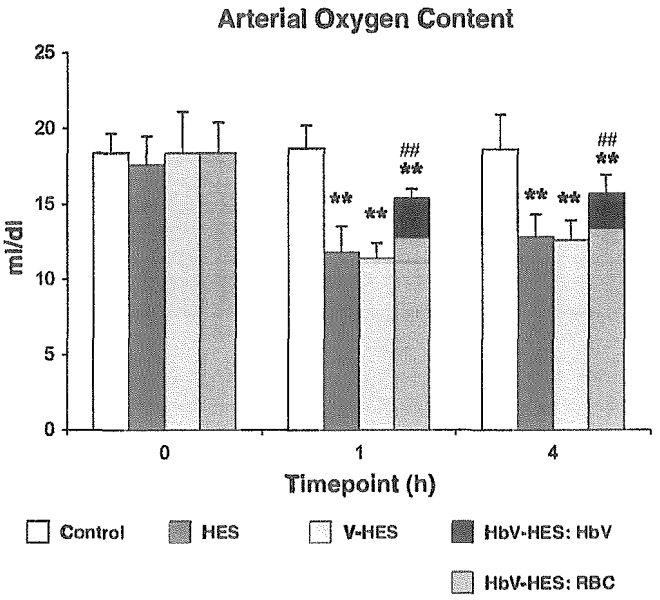

Fig. 1. Oxygen content in carotid artery at baseline and 1 and 4 h after hemodilution with 6% hydroxyethyl starch (HES) and vesicles with (HbV-HES) and without (V-HES) Hb suspended in HES, including relative contribution of red blood cells (RBCs) and HbV. Data are given as percentages of baseline and represent means ± SD. $^{**}P < 0.01$ vs. baseline; $\#\#P < 0.01$ vs. other groups.

At baseline, the microvascular diameters were 42 ± 17 μm for conduit arterioles, 10.6 ± 3.5 μm for end arterioles, and 88 ± 14 μm for venules. In both flap areas and in all groups, the diameters were similar at baseline and they remained virtually unchanged throughout the experiments.

The behavior of the capillary hemodynamics in both parts of the flap is shown in Fig. 2. At baseline, the capillaries in the ischemic tissue were significantly wider than the anatomically perfused capillaries (means of 3.31–3.33 vs. 2.79–2.82 μm; $P < 0.01$). In the control group, the capillaries further dilated over time in both the anatomically perfused and the ischemic tissue by 25% and 9%, respectively (both $P < 0.01$). This time-related dilation was significantly attenuated in all hemodiluted animals ($P < 0.01$ vs. control), the most pronounced after HbV-HES, which resulted in a reduction of capillary diameter in the ischemic tissue to values close to baseline values obtained in the anatomically perfused tissue (2.85 ± 0.03 μm; $P < 0.01$ vs. baseline and other groups). The induction of ischemia reduced capillary RBC velocity by ~60% ($P < 0.01$). Hemodilution increased RBC velocity by ~50% in the anatomically perfused tissue and ~150% in the ischemic tissue (both $P < 0.01$ vs. baseline and control) for all diluents, whereas RBC velocity further declined in the ischemic tissue of the control animals over time by 67% ($P < 0.01$). In the ischemic tissue, baseline FCD was ~50% lower than in the anatomically perfused tissue ($P < 0.01$). In the control group, FCD decreased to 85% of baseline in the anatomically perfused tissue and to 69% in the ischemic tissue over time (both $P < 0.01$), whereas hemodilution kept FCD at baseline levels in the anatomically perfused tissue ($P < 0.01$ vs. control) and increased FCD in the ischemic tissue by 31% after HES ($P < 0.01$ vs. other groups), 66% after V-HES, and 62% after HbV-HES (all $P < 0.01$ vs. baseline). At baseline, the calculated RBC perfusion index in the ischemic tissue was reduced to ~20% of the value obtained in the anatomically perfused tissue ($P < 0.01$), and it was further decreased in both tissues of the control animals over time ($P < 0.01$). Hemodilution raised the RBC perfusion index by ~50% in the anatomically perfused tissue, independently of the diluent given ($P < 0.01$ vs. baseline and control), and by 186% after HES ($P < 0.01$ vs. other groups), 330% after V-HES, and 316% after HbV-HES in the ischemic tissue (all $P < 0.01$ vs. baseline and control; P = not significant between vesicle groups).

The baseline macromolecular leakage was slightly increased in the ischemic tissue compared with the anatomically perfused part (not significant; Fig. 3). In the control and HES groups, macromolecular leakage was increased by 20–30% in both parts of the flap over time ($P < 0.01$ for anatomical; $P < 0.05$ for ischemic), whereas it remained virtually unchanged after hemodilution with the vesicle solutions ($P < 0.01$ vs. control and HES).

The baseline mean Po_2 ranged from 22.7 to 25.2 mmHg in the anatomically perfused tissue and was significantly reduced in the ischemic tissue to 10.2–10.8 mmHg ($P < 0.01$; Fig. 4). The values remained at baseline levels in both parts of the flap and in all groups except for HbV-HES, which led to a significant Po_2 increase to 16.0 ± 1.8 mmHg in the ischemic tissue ($P < 0.01$ vs. baseline and other groups).

A massive accumulation of TUNEL-positive nuclei was observed in the ischemic tissue of untreated animals (Fig. 5). Compared with the anatomically perfused tissue, a 2-fold increase was counted in the dermis and a 1.5-fold increase in the epidermis (Fig. 6; both $P < 0.01$), which were both partly attenuated by diluting the animals with HES and V-HES (both $P < 0.01$ vs. control) and completely abolished after HbV-HES, which also revealed significantly lower counts in the anatomically perfused tissue ($P < 0.01$ vs. other groups).

DISCUSSION

This study was designed to determine the relevance of Hb supplemented as an oxygen carrier to a solution used for isovolemic hemodilution with the scope of improving oxygenation in critically ischemic tissue, as previously described (8, 12). This was made possible by direct comparison of the oxygen-carrying solution with a solution void of oxygen carriers but with otherwise absolutely identical physicochemical properties, a constellation that, to our knowledge, has not yet been investigated. Our findings revealed that the presence of Hb in the vesicles administered in the course of isovolemic hemodilution was essential to significantly attenuate both hypoxia and subsequent cell death in the critically ischemic tissue, which were restored to values in the range of those found in the anatomically perfused tissue.

However, some benefit in tissue survival could also be obtained with the diluents void of oxygen carriers, which was related to a substantial improvement in all capillary hemodynamic parameters, and which was more pronounced in the compromised microcirculation in the ischemic tissue. The level of hemodilution we chose is considered to yield the maximal RBC flux at the capillary level (20). However, compared with HES, the improvement in capillary hemodynamics in the ischemic tissue was further enhanced by adding vesicles to the solution, which resulted in a significant increase in plasma

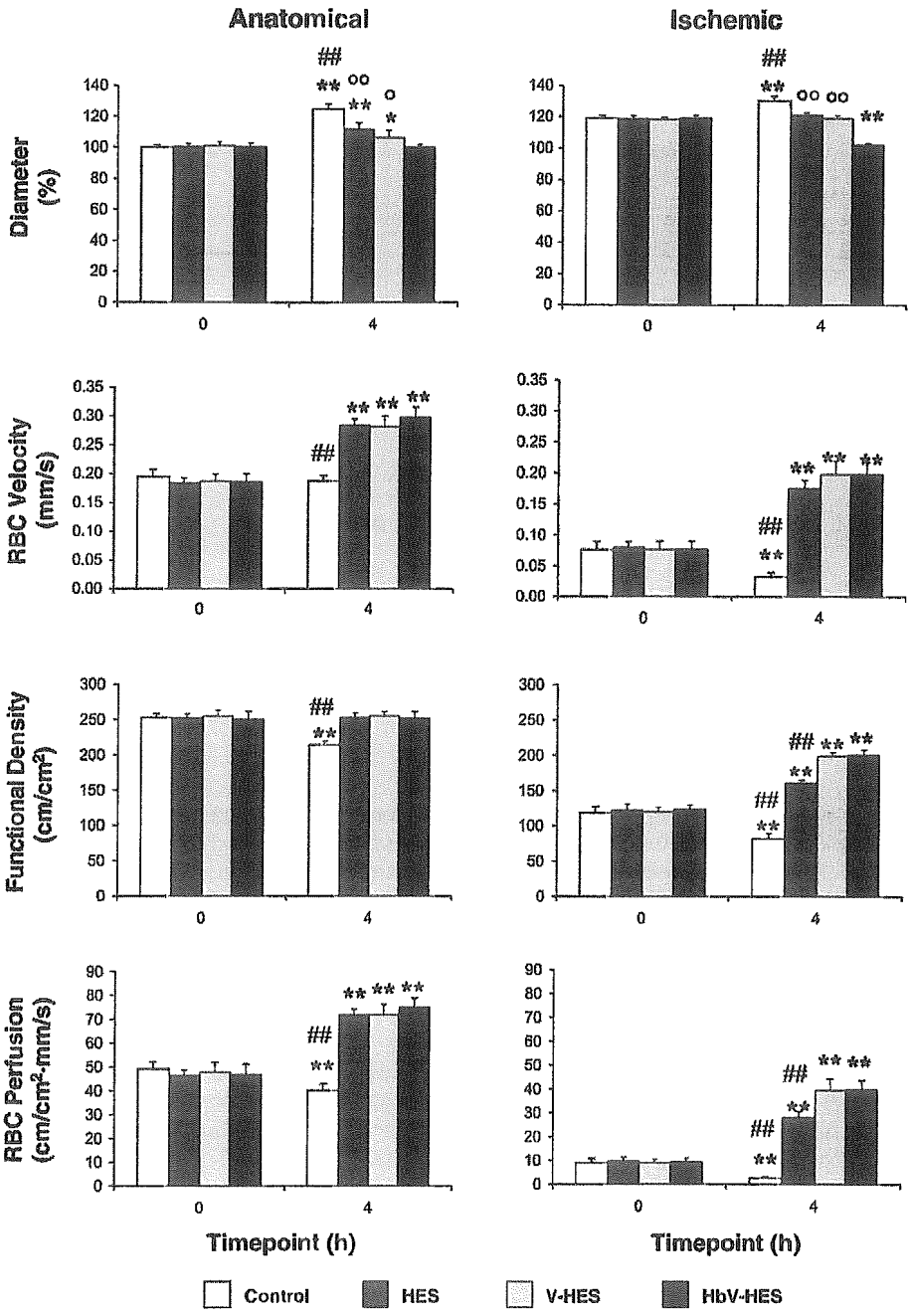

Fig. 2. Capillary hemodynamics in anatomically perfused and ischemic tissues at baseline and 4 h after hemodilution with 6% HES, HbV-HES, and V-HES. Data represent means ± SD. Values for capillary diameter were expressed in percentages of mean in anatomically perfused tissue of control animals at baseline. $^{*}P < 0.05$, $^{**}P < 0.01$ vs. baseline; $\#\#P < 0.01$ vs. other groups; $^{\circ}P < 0.05$, $^{\circ\circ}P < 0.01$ vs. HbV-HES.

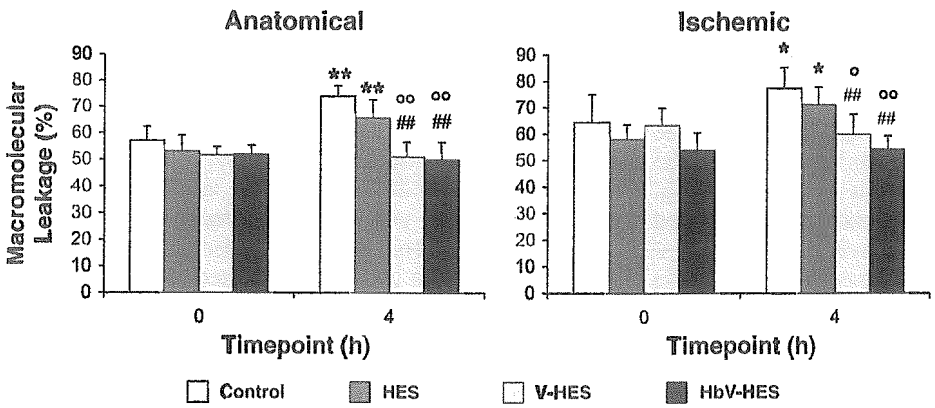

Fig. 3. Macromolecular leakage in anatomically perfused and ischemic tissues at baseline and 4 h after hemodilution with 6% HES, HbV-HES, and V-HES. Data represent means ± SD. $^{*}P < 0.05$, $^{**}P < 0.01$ vs. baseline; $\#\#P < 0.01$ vs. control; $^{\circ}P < 0.05$, $^{\circ\circ}P < 0.01$ vs. HES.

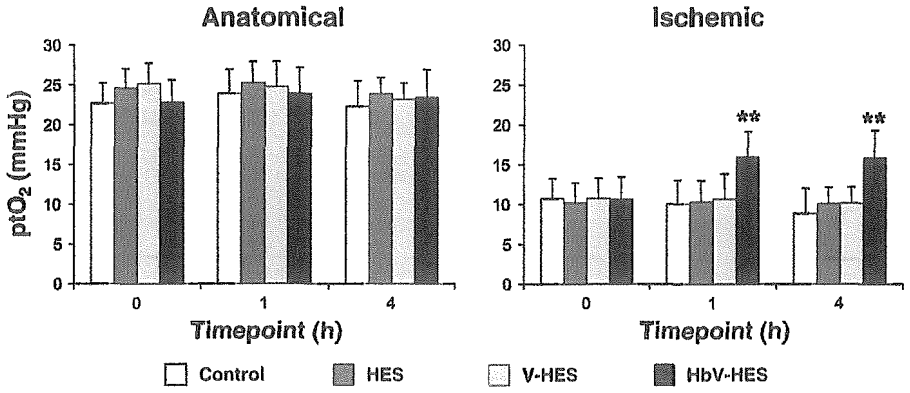

Fig. 4. Partial tissue oxygen tension (P_tO_2) in anatomically perfused and ischemic tissues at baseline and 1 and 4 h after hemodilution with 6% hydroxyethyl starch (HES), HbV-HES, and V-HES. Data represent means ± SD. $^{**}P < 0.01$ vs. baseline and other groups.

viscosity. A dependency of FCD on plasma viscosity has been described for conditions of severe hemodilution (2, 3, 33), which has been ascribed to shear stress-induced, nitric oxide-mediated arteriolar vasodilation being required to maintain capillary pressurization (2, 3, 9). However, during the moderate hemodilution applied in the present study, no such arteriolar vasodilation could be observed, which calls for alternative explanations not only for the behavior of FCD but also of capillary RBC velocity and perfusion.

One interpretation may be found in the changes in macromolecular leakage. This parameter allows for a quantitative assessment of capillary leakage, which is an early sign of inflammation appearing in the course of compromised microcirculation such as that due to trauma (31), hemorrhagic shock (5), or ischemia-reperfusion injury (18), and which is paralleled by the activation of the leukocyte-endothelium interaction particularly in the postcapillary venules. Leukocyte adherence, being an early step in this cascade of events, may augment resistance in this vascular segment considerably and thus impair capillary hemodynamics in critically perfused tissues (19). Compared with both the control group and the HES group, macromolecular leakage was significantly reduced in the animals receiving vesicles. Therefore, it may be postulated that the beneficial effect of the vesicles on the capillary hemodynamics was related to a reduction of postcapillary resistance in terms of blunting leukocyte adherence. The capability of leukocytes to adhere to the endothelial wall may be diminished by increasing shear stress (21), which is proportional to linear flow velocity and viscosity of the plasma and inversely proportional to vascular diameter. Provided that our data on plasma viscosity and capillary hemodynamics may be extrapolated to the conditions in the ischemic postcapillary

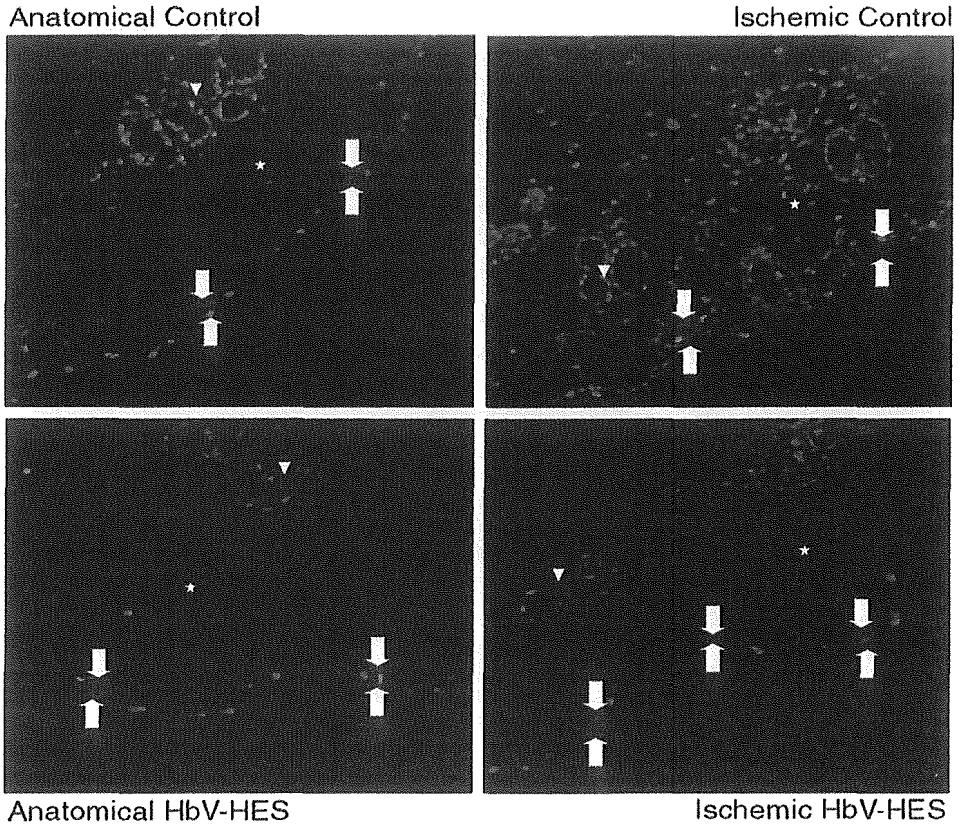

Fig. 5. Transferase-mediated dUTP nick-end labeling (TUNEL) assay of apoptotic cells in anatomically perfused and ischemic tissues 5 h after completion of surgery and 4 h after hemodilution with HbV-HES. Note massive accumulation of red-labeled apoptotic cells in both dermis (☆) and epidermis (arrows) of ischemic tissue and how apoptosis was reduced after hemodilution with HbV-HES. Hair follicles and sebaceous glands are shown (arrowheads).

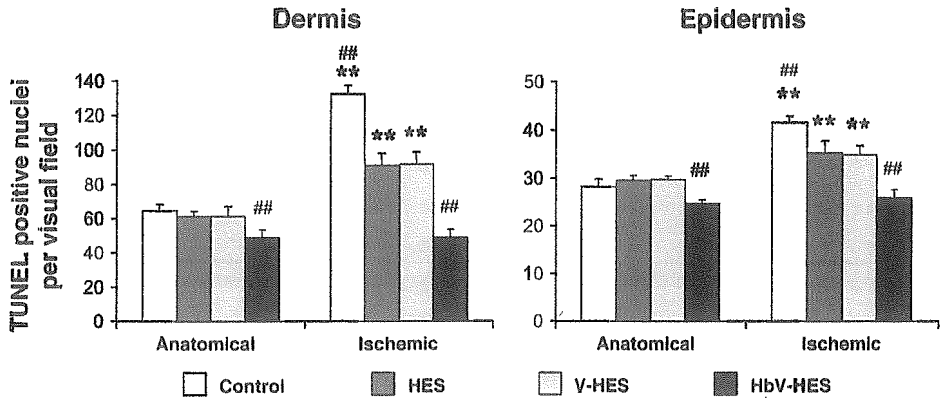

Fig. 6. Density of apoptotic cells in dermis and epidermis of anatomically perfused and ischemic tissues 5 h after completion of surgery and 4 h after hemodilution with 6% HES, HbV-HES, and V-HES. Data represent means ± SD. $^{**}P < 0.01$ vs. anatomically perfused tissue; $^{\#\#}P < 0.01$ vs. other groups.

venules, hemodilution with the vesicle solutions would result in a significant shear stress increase in these vessels compared with baseline and HES, respectively. This mechanism may be of a particular importance in case of ischemia-reperfusion injury after reoxygenation of critically ischemic tissue (16), which may, at least partly, have taken place in the animals receiving HbVs, as evidenced by the improved partial tissue oxygen tension.

In the present preparation, macromolecular leakage appeared to be primarily related to the traumatization of the tissue as a consequence of its surgical manipulation (7), because similar values were obtained in both parts of the flap. However, it is conceivable that the ischemic tissue is more susceptible to changes in postcapillary resistance because of the diminished driving pressure in the collateralized arterioles that are nourished by connecting arterioles, in which perfusion pressures below 30 mmHg were measured, compared with ~45 mmHg in the arterioles feeding the anatomically perfused vasculature (3, 10). With regard to the postulated effect of the vesicles on the postcapillary resistance, this would explain why the vesicle-related improvement of capillary hemodynamics was restricted to the ischemic tissue. Moreover, the vesicle-related increase in capillary perfusion coincided with a decrease in capillary diameters. Given the assumption that the perfusion increase was caused by a reduction of upstream vascular resistance, this would have led to capillary dilation as a result of increased intraluminal capillary pressure (3), whereas intraluminal capillary pressure decreases if vascular resistance is diminished on the postcapillary level. Therefore, the inversely proportional behavior of capillary diameter and perfusion further supports our assumption that the microhemodynamic benefit obtained with the vesicle solutions was predominantly due to its reduction of postcapillary resistance.

Although all capillary hemodynamic parameters in the ischemic tissue were restored to values close to baseline in the anatomically perfused tissue in the V-HES group, this was not sufficient to attenuate hypoxia or hypoxia-induced apoptosis. This suggests that in this group, oxygen delivery to the ischemic tissue is reduced because of a lack of oxygen content in its collateralized, arteriolar inflow, a condition that was presumably circumvented by the presence of Hb in the vesicles because of various reasons. First, the HbVs contribute to a total Hb increase, thus resulting in an enhanced oxygen-carrying capacity not only in terms of arterial oxygen content but also in terms of additional capillary, HbV-related oxygen flow that is not included in the index used to express capillary perfusion in the present study. Second, the high oxygen affinity of the HbVs may have attenuated the unloading of oxygen in the upstream vasculature before reaching the collateralized arterioles, which has been estimated to be as much as 40–50% of the systemic arterial oxygen content (11, 30). This hypothesis is supported by both experimental (15, 25, 30) and theoretical (34) studies, which showed that oxygen delivery may be shifted to the downstream direction if oxygen carriers with high oxygen affinity were infused. Third, because of their small size, HbVs may perfuse capillaries in the compromised microcirculation that are no longer accessible by RBCs. Indeed, HbVs were observed in capillaries showing a cessation of RBC flux (29), which would virtually enhance the density of functional capillaries. Moreover, the occurrence of apoptosis leads to a reduction of oxygen consumption, thus raising partial tissue oxygen tension, provided oxygen delivery remains unchanged. Therefore, the partial tissue oxygen tension increase observed after HbV-HES may underestimate the improvement in oxygen delivery in comparison with the other groups.

In summary, on the basis of the unique constellation in which a HbV solution was compared with a nonoxygen-carrying vesicle solution with identical physicochemical properties, we conclude that the presence of Hb in the vesicles is necessary to obtain an essential improvement of oxygenation and survival in the critically ischemic flap tissue. However, the benefit may, to a certain extent, be ascribed to the rheological changes provided by the vesicles, presumably by reducing postcapillary vascular resistance.

ACKNOWLEDGMENTS

We greatly acknowledge Prof. S. Takeoka and Dr. K. Sou (Advanced Research Institute for Science and Engineering, Waseda University, Tokyo, Japan) for the preparation of the phospholipid vesicles, and Prof. A. C. Andres and V. Rohrbach (Department of Clinical Research, Inselspital University Hospital, Bern, Switzerland) for assistance in the immunohistochemical analysis.

GRANTS

This research was supported by the Swiss National Foundation for Scientific Research Grants 32–054092.98 and 32–065149.01 (to D. Erni) and 32–050771.97 (to M. Leunig), by the Department of Clinical Research, University of Berne, Switzerland, and by Health Sciences Research (Research on Regulatory Science Grant H16-IYAKU-069, 071) from the Ministry of Health, Labour and Welfare, Japan, and Grants-in-Aid for Scientific Research from the Japan Society for the Promotion of Science (B-16300162).

REFERENCES

1. **Ansari B, Coates PJ, Greenstein BD, and Hall PA.** In situ end-labeling detects DNA strand breaks in apoptosis and other physiological and pathological states. *J Pathol* 170: 1–8, 1993.
2. **Bertuglia S.** Increased viscosity is protective for arteriolar endothelium and microvascular perfusion during severe hemodilution in hamster cheek pouch. *Microvasc Res* 61: 56–63, 2001.
3. **Cabrales P, Tsai AG, and Intaglietta M.** Microvascular pressure and functional capillary density in extreme hemodilution with low- and high-viscosity dextran and a low-viscosity Hb-based O_2 carrier. *Am J Physiol Heart Circ Physiol* 287: H363–H373, 2004.
4. **Chang TM.** Artificial cells for cell and organ replacements. *Artif Organs* 28: 265–270, 2004.
5. **Childs EW, Udobi KF, and Hunter FA.** Hypothermia reduces microvascular permeability and reactive oxygen species expression after hemorrhagic shock. *J Trauma* 58: 271–277, 2005.
6. **Chowdary RP, Berkower AS, Moss ML, and Hugo NE.** Fluorocarbon enhancement of skin flap survival in rats. *Plast Reconstr Surg* 79: 98–101, 1987.
7. **Contaldo C, Plock JA, Djonov V, Leunig M, Banic A, and Erni D.** The influence of trauma and ischemia on carbohydrate metabolites monitored in hamster flap tissue. *Anesth Analg*: 817–822, 2005.
8. **Contaldo C, Schramm S, Wettstein R, Sakai H, Takeoka S, Tsuchida E, Leunig M, Banic A, and Erni D.** Improved oxygenation in ischemic hamster flap tissue is correlated with increasing hemodilution with Hb vesicles and their O_2 affinity. *Am J Physiol Heart Circ Physiol* 285: H1140–H1147, 2003.
9. **de Wit C, Schafer C, von Bismarck P, Bolz SS, and Pohl U.** Elevation of plasma viscosity induces sustained NO-mediated dilation in the hamster cremaster microcirculation in vivo. *Pflügers Arch* 434: 354–361, 1997.
10. **Erni D, Sakai H, Banic A, Tschopp H, and Intaglietta M.** Quantitative assessment of microhemodynamics in ischemic skin flap tissue by intravital microscopy. *Ann Plast Surg* 43: 405–415, 1999.
11. **Erni D, Sakai H, Tsai AG, Banic A, Sigurdsson GH, and Intaglietta M.** Haemodynamics and oxygen tension in the microcirculation of ischaemic skin flaps after neural blockade and haemodilution. *Br J Plast Surg* 52: 565–572, 1999.
12. **Erni D, Wettstein R, Schramm S, Contaldo C, Sakai H, Takeoka S, Tsuchida E, Leunig M, and Banic A.** Normovolemic hemodilution with Hb vesicle solution attenuates hypoxia in ischemic hamster flap tissue. *Am J Physiol Heart Circ Physiol* 284: H1702–H1709, 2003.
13. **Faithfull NS, Fennema M, and Erdmann W.** Protection against myocardial ischaemia by prior haemodilution with fluorocarbon emulsions. *Br J Anaesth* 60: 773–778, 1988.
14. **Fitzpatrick CM, Savage SA, Kerby JD, Clouse WD, and Kashyap VS.** Resuscitation with a blood substitute causes vasoconstriction without nitric oxide scavenging in a model of arterial hemorrhage. *J Am Coll Surg* 199: 693–701, 2004.
15. **Intaglietta M.** Microcirculatory basis for the design of artificial blood. *Microcirculation* 6: 247–258, 1999.
16. **Kajimura M, Ichikawa M, Sakai H, Takeoka S, Tsuchida E, and Suematsu M.** Real time imaging of anionic liposome during thrombus formation and acute inflammation in rats (Abstract). In: *2nd Japan-United Kingdom Platelet Conference, Oxford, UK, 2004*. London: Br Soc for Haemostasis and Thrombosis, 2004.
17. **Klyscz T, Jünger M, Jung F, and Zeintl H.** Cap image–A new kind of computer-assisted video image analysis system for dynamic capillary microscopy. *Biomed Tech* 42: 168–175, 1997.
18. **Menger MD, Pelikan S, Steiner D, and Messmer K.** Microvascular ischemia-reperfusion injury in striated muscle: significance of "reflow paradox." *Am J Physiol Heart Circ Physiol* 263: H1901–H1906, 1992.
19. **Menger MD, Steiner D, and Messmer K.** Microvascular ischemia-reperfusion injury in striated muscle: significance of "no reflow." *Am J Physiol Heart Circ Physiol* 263: H1892–H1900, 1992.
20. **Mirhashemi S, Ertefai S, Messmer K, and Intaglietta M.** Model analysis of the enhancement of tissue oxygenation by hemodilution due to increased microvascular flow velocity. *Microvasc Res* 34: 290–301, 1987.
21. **Moazzam F, DeLano FA, Zweifach BW, and Schmid-Schönbein GW.** The leukocyte response to fluid stress. *Proc Natl Acad Sci USA* 94: 4825–4827, 1997.
22. **Piston DW.** Choosing objective lenses: the importance of numerical aperture and magnification in digital optical microscopy. *Biol Bull* 195: 1–4, 1998.
23. **Powanda DD and Chang TM.** Cross-linked polyhemoglobin-superoxide dismutase-catalase supplies oxygen without causing blood-brain barrier disruption or brain edema in a rat model of transient global brain ischemia-reperfusion. *Artif Cells Blood Substit Immobil Biotechnol* 30: 23–37, 2002.
24. **Premaratne S, Harada RN, Chun P, Suehiro A, and McNamara JJ.** Effect of perfluorocarbon exchange transfusion on reducing myocardial infarct size in a primate model of ischemia-reperfusion injury: a prospective, randomized study. *Surgery* 117: 670–676, 1995.
25. **Sakai H, Cabrales P, Tsai AG, Tsuchida E, and Intaglietta M.** Oxygen release from low and normal P_{50} Hb vesicles in transiently occluded arterioles of the hamster window model. *Am J Physiol Heart Circ Physiol* 288: H2897–H2903, 2005.
26. **Sakai H, Hara H, Yuasa M, Tsai AG, Takeoka S, Tsuchida E, and Intaglietta M.** Molecular dimensions of Hb-based O_2 carriers determine constriction of resistance arteries and hypertension. *Am J Physiol Heart Circ Physiol* 279: H908–H915, 2000.
27. **Sakai H, Masada Y, Horinouchi H, Ikeda E, Sou K, Takeoka S, Suematsu M, Takaori M, Kobayashi K, and Tsuchida E.** Physiological capacity of the reticuloendothelial system for the degradation of hemoglobin vesicles (artificial oxygen carriers) after massive intravenous doses by daily repeated infusions for 14 days. *J Pharmacol Exp Ther* 311: 874–884, 2004.
28. **Sakai H, Masada Y, Horinouchi H, Yamamoto M, Ikeda E, Takeoka S, Kobayashi K, and Tsuchida E.** Hemoglobin-vesicles suspended in recombinant human serum albumin for resuscitation from hemorrhagic shock in anesthetized rats. *Crit Care Med* 32: 539–545, 2004.
29. **Sakai H, Takeoka S, Wettstein R, Tsai AG, Intaglietta M, and Tsuchida E.** Systemic and microvascular responses to hemorrhagic shock and resuscitation with Hb vesicles. *Am J Physiol Heart Circ Physiol* 283: H1191–H1199, 2002.
30. **Sakai H, Tsai AG, Rohlfs RJ, Hara H, Takeoka S, Tsuchida E, and Intaglietta M.** Microvascular response to hemodilution with Hb vesicles as red blood cell substitutes: influence of O_2 affinity. *Am J Physiol Heart Circ Physiol* 276: H552–H562, 1999.
31. **Schaser KD, Vollmar B, Menger MD, Schewior L, Kroppenstedt SN, Raschke M, Lubbe As Haas NP, and Mittlmeier T.** In vivo analysis of microcirculation following closed soft-tissue injury. *J Orthop Res* 17: 678–685, 1999.
32. **Sutherland GR, Farrar JK, and Peerless SJ.** The effect of Fluosol-DA on oxygen availability in focal cerebral ischemia. *Stroke* 15: 829–835, 1984.
33. **Tsai AG, Friesenecker B, McCarthy M, Sakai H, and Intaglietta M.** Plasma viscosity regulates capillary perfusion during extreme hemodilution in hamster skinfold model. *Am J Physiol Heart Circ Physiol* 275: H2170–H2180, 1998.
34. **Vadapalli A, Goldman D, and Popel AS.** Calculations of oxygen transport by red blood cells and hemoglobin solutions in capillaries. *Artif Cells Blood Substitut Immobil Biotechnol* 30: 157–188, 2002.

Human Serum Albumin Bearing Covalently Attached Iron(II) Porphyrins as O_2-Coordination Sites

Rong-Min Wang,[†,‡] Teruyuki Komatsu,[†] Akito Nakagawa,[†] and Eishun Tsuchida*[,†]

Advanced Research Institute for Science and Engineering, Waseda University, 3-4-1 Okubo, Shinjuku-ku, Tokyo 169-8555, Japan, and Institute of Polymer, Northwest Normal University, Lanzhou 730070, China . Received June 17, 2004; Revised Manuscript Received September 25, 2004

Tetrakis{(α,α,α,α-*o*-pivalamido)phenyl}porphinatoiron(II) with a bifunctional tail possessing an axially coordinated imidazolyl group and a protein attachable succinimidyl(glutamyl) group (FeP-GluSu) has been synthesized. It can efficiently react with the lysine residues of recombinant human serum albumin (rHSA), giving a new albumin–heme conjugate [rHSA(FeP-Glu)]. MALDI-TOFMS showed a distinct molecular ion peak at *m/z* 70 643, which indicates that three FeP-Glu molecules were covalently linked to the rHSA scaffold. The binding number of FeP-Glu is approximately three (mol/mol) and independent of the mixing ratio. The CD spectrum and Native PAGE revealed that the albumin structure remained unaltered after the covalent bonding of the hemes. This rHSA(FeP-Glu) conjugate can bind and release O_2 reversibly under physiological conditions (pH 7.3, 37 °C) in the same manner as hemoglobin and myoglobin. The O_2-adduct complex had a remarkably long lifetime ($\tau_{1/2}$: 5 h). The O_2-binding affinity [$P_{1/2}{}^{O_2}$: 27 Torr] was identical to that of human red cells. Laser flash photolysis experiments gave the O_2- and CO-association rate constants and suggested that there are two different geometries of the imidazole binding to the central ion.

Human serum albumin (HSA), which is the major plasma protein component in our bloodstream, has no prosthetic group; however it nonspecifically captures many endogenous and exogenous compounds by weak interactions, *e.g.,* H-bond, ionic attraction, and hydrophobic interaction, namely noncovalent bonds (*1*–*3*). Synthetic heme, 2-[{8-*N*-(2-methylimidazolyl)octanoyl}-oxy]methyl-5,10,15,20-tetrakis{(α,α,α,α-*o*-pivalamido)-phenyl}porphinatoiron(II) (FeP, Chart 1 a) is also incorporated into recombinant HSA (rHSA), and the obtained albumin–heme (rHSA-FeP) hybrid can reversibly coordinate O_2 under physiological conditions (pH 7.3, 37 °C) (*4*). This O_2-carrying plasma hemoprotein could be of medical importance as a blood replacement composition (*4e*–*g*). Nevertheless, the major driving force of the heme-binding to albumin is a hydrophobic interaction; therefore, its binding constants (10^4–10^6 M^{-1}) are not high enough to maintain the heme concentration in the circulatory system for a long period (*4a*). The administration of the albumin–heme hybrid solution into rats demonstrated that the lifetimes of the heme was less than 6 h (*4e, 5*). To immobilize the heme group to the albumin scaffold more tightly and retain its O_2-transport efficacy, we have combined the O_2-coordination site FeP to the rHSA structure through a covalent bond. In this communication, we report, for the first time, the synthesis of a novel FeP analogue with a bifunctional branched-tail including an axially coordinated imidazolyl group and a protein-attachable succinimidyl(glutamyl) group (FeP-GluSu, Chart 1 a), and the properties of the rHSA conjugate bearing covalently linked FeP-Glu as a new O_2-carrying hemoprotein.

Chart 1. (a) 5,10,15,20-Tetrakis{(α,α,α,α-*o*-pivalamido)-phenyl}porphinatoiron Derivatives with a Bifunctional Tail Group. (b) Space-Filling Representation of the Oxygenated FeP-GluSu by Insight II (see ref 11)

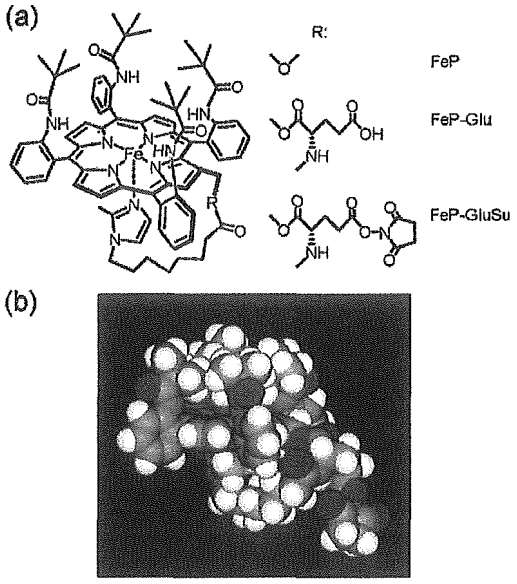

As a functional side-chain of FeP, which directly makes a covalent bond to rHSA, we selected the succinimidyl group, because it selectively reacts with the NH_2 group of lysine in the range of pH 6.3–8.6 with high yield. The branched tail that includes the imidazolyl and succnimidyl groups via a glutamate junction was introduced into the parent porphyrin **1** (*6*) as shown in Scheme 1 (*7*).

* Corresponding author. Phone: +81 3-5286-3120. Fax: +81-3-3205-4740. E-mail: eishun@waseda.jp.
† Waseda University.
‡ Northwest Normal University.

10.1021/bc049859m CCC: $30.25
Published on Web 11/12/2004

Scheme 1. Synthetic Scheme of FeP-GluSu

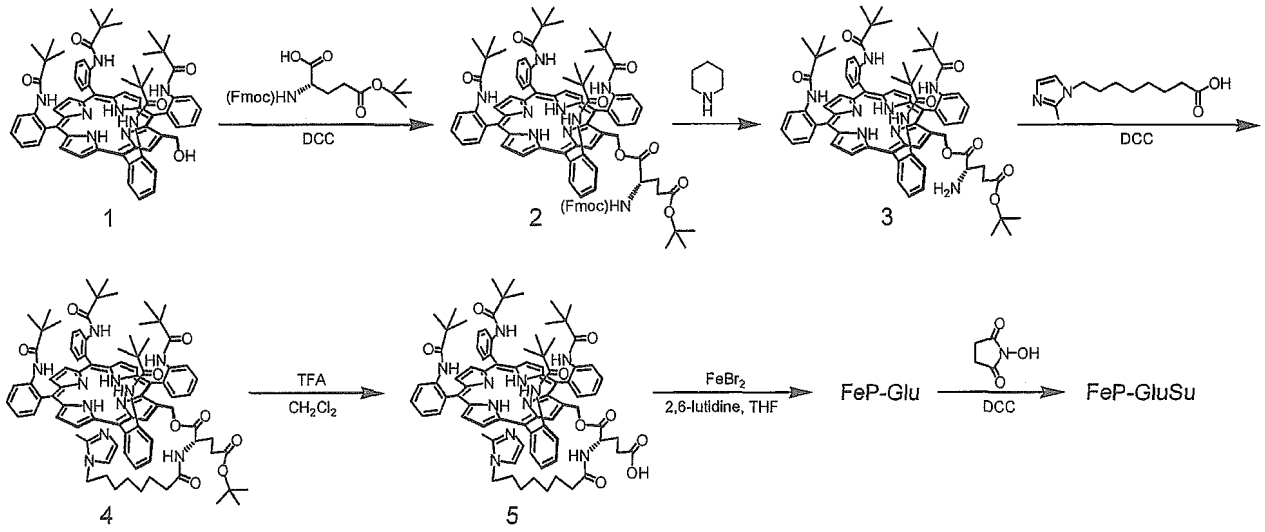

Table 1. CO-and O_2-Binding Parameters of rHSA(FeP-Glu) Conjugate in Phosphate–Buffered Solution (pH 7.3) at 25 °C

	$10^{-6}\,k_{on}^{CO}(M^{-1}\,s^{-1})$		$10^{-7}\,k_{on}^{O_2}(M^{-1}\,s^{-1})$		$10^{-2}\,k_{off}^{O_2}(s^{-1})$		$P_{1/2}^{O_2}$(Torr)[a]
system	fast	slow	fast	slow	fast	slow	
rHSA(FeP-Glu) conjugate	6.2	1.1	2.8	–	3.3	–	9 (27)
rHSA-FeP hybrid[b]	4.7	0.66	3.2	1.0	7.2	2.2	13 (35)
Hb(T-state)α[c]	0.22	–	0.29	–	1.8	–	40

[a] At 37 °C in parenthesis. [b] From ref 4c. [c] From refs 13–15.

First, Fmoc-L-Glu(g-*tert*-butyl ester) was bound to the OH group at the β-pyrrolic position of the porphyrin **1** by DCC. After removal of the Fmoc protecting group with piperidine, 8-*N*-(2-methylimidazolyl)octanoic acid was reacted with the obtained compound **3** in CH_2Cl_2, giving the imidazolyl-tailed porphyrin (**4**). The *tert*-butyl group was then removed by TFA, and the central iron insertion was carried out by the general $FeBr_2$ method to afford the iron-porphryin FeP-Glu. Finally, the reaction of *N*-hydroxysuccinimide with DCC gave the FeP-GluSu. All reactions can be performed at room temperature with high yields. The analytical data of all compounds described above were satisfactory obtained (*7*).

The FeP-Glu was converted to the ferrous complex by reduction in a heterogeneous two-phase system (toluene/aqueous $Na_2S_2O_4$) under an N_2 atmosphere (*6, 8*). The UV–vis absorption spectrum of the orange solution showed five-*N*-coordinated Fe(II) species (λ_{max}: 440, 531, 563 nm) via intramolecular imidazole binding (*6, 8, 9*). Upon exposure to CO, its UV–vis absorption immediately moved to that of the CO adduct complex. On the other hand, the dioxygenation was unstable at 25 °C, which is likely due to the presence of the neighboring glutamic acid proton.

The EtOH solution of the carbonyl FeP-GluSu (2 mL) was then injected into the phosphate-buffered solution of rHSA (8 mL, pH 7.3) (molar ratio 4/1), and the mixture was gently stirred for 1 h at room temperature. The solution was dialyzed against phosphate buffer (pH 7.3) to remove EtOH. The MALDI-TOFMS demonstrated a single molecular ion peak at *m/z* 70 643 (Figure 1). Attempts to measure the molecular weight of the rHSA-FeP hybrid, in which the FePs are noncovalently accommodated, failed using MALDI- and ESI-TOFMS; the molecular ion peak of rHSA (65 500) was only observable because the FePs are dissociated from the albumin during the ionization process (*10*). Therefore, we can conclude that the FeP-Glu is conjugated with rHSA

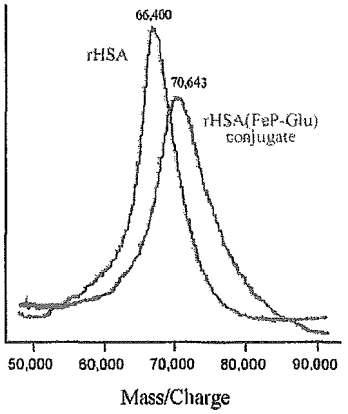

Figure 1. MALDI-TOFMS of the rHSA(FeP-Glu) conjugate. Matrix: 2,5-dihydroxybenzoic acid.

through amide bond formation. The average number of FeP-Glu in an rHSA was estimated to be 2.9–3.5, and this number is not dependent on the mixing molar ratio of FeP-GluSu/rHSA that ranged from 4 to 10. There are a total of 59 NH_2 groups in the rHSA structure, but only three of them are presumably active for the FeP-GluSu binding.

The conjugation of FeP-GluSu did not induce any change in the circular dichroism spectrum of rHSA in the 200–250 nm region. The Native PAGE of rHSA(FeP-Glu) also showed a single band with same migration distance of rHSA. Both results suggested that the secondary structure, molecular shape, and surface charge of albumin remained unaltered after the covalent binding of the hemes.

The UV–vis absorption spectrum of the rHSA(FeP-Glu) conjugate under an N_2 atmosphere showed a typical five-*N*-coordinated complex as seen in the toluene solution of FeP-Glu (Figure 2) (*4a,b, 6, 8, 9*). Upon exposure

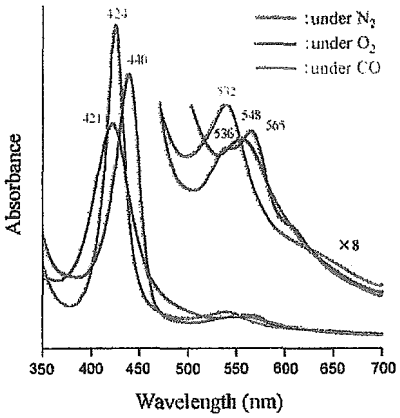

Figure 2. UV–vis absorption spectral changes of the rHSA-(FeP-Glu) conjugate in phosphate-buffered solution (pH 7.3) at 25 °C.

of this solution to O_2, the spectrum changed to that of the O_2-adduct complex under physiological conditions (pH 7.3, 37 °C) (*4a–c*). This dioxygenation was reversibly observed to be dependent on the O_2 partial pressure in the same manner as hemoglobin (Hb) and myoglobin. The half-lifetime of the O_2 adduct (ca. 5 h at 37 °C) was significantly longer than that of the noncovalent rHSA-FeP hybrid ($\tau_{1/2}$: 2 h) (*4d*). The covalent linkages of FeP-Glu to the protein scaffold obviously retarded the oxidation process of the central ferrous ion. Molecular simulation of the structure of FeP-GluSu revealed that the geometry of the imidazole ring against the porphyrin platform was perpendicular, which suggests that the spacer moiety between the imidazole and the porphyrin periphery does not produce an unfavorable distortion of the axial coordination and will not influence the O_2-binding behavior (see Chart 1b) (*11*).

The O_2-binding affinity [$P_{1/2}{}^{O_2}$] of the rHSA(FeP-Glu) conjugate was determined to be 27 Torr at 37 °C (*3b,c, 6, 7, 9, 10*), which is almost the same as that of the rHSA-FeP hybrid [$P_{1/2}{}^{O_2}$: 33 Torr] (*3b–d*) and identical to that of human red cells (*12*). The laser flash photolysis experiments provided the association rate constants of the O_2- and CO-bindings ($k_{on}{}^{O_2}$, $k_{on}{}^{CO}$) (*6, 8, 9a*). The absorption decays accompanying the O_2- and CO-recombination to the noncovalent rHSA-FeP hybrid were composed of two phases of the first-order kinetics, and the curves were fit by a double-exponential equation to determine k_{on} (fast) and k_{on} (slow) (Table 1) (*4c*). We supposed that the O_2- and CO-association to the FeP in the hydrophobic domains of the albumin was influenced by the molecular microenvironments around each O_2-coordination site, e.g., steric hindrance of the amino acid residue and difference in polarity (*4b–d*). The time dependence of the absorption change in the CO recombination to the rHSA(FeP-Glu) conjugate also showed double-exponential profile, but the rebinding process of O_2 obeyed monophasic decay. On the basis of studies on synthetic model hemes, it has been known that the proximal-side effect is the only primary factor which influences the association rate for CO but not for O_2 (*8, 9a*). We assume that there are two different geometries of the imidazole coordination and that each one shows the individual kinetics of the CO association. The covalent linkages between the axially coordinated imidazolyl side-chain and the albumin structure may provide an additional strain of the Fe–N(imidazole) bond and gives two conformations of the proximal-base binding. Since the $k_{on}{}^{O_2}$ value of rHSA(FeP-Glu) was nearly the same as the $k_{on}{}^{O_2}$ (fast) of the rHSA-FeP hybrid (Table 1), the FeP-Glu molecules are likely to locate on the surface of rHSA.

In conclusion, reaction of the newly synthesized tetrakis{(α,α,α,α-*o*-pivalamido)phenyl}porphinatoiron(II) with a proximal base and succinimidyl(glutamyl) group to rHSA produced a novel albumin conjugate bearing covalently attached heme groups as O_2-coordination sites. The molecular weight of rHSA(FeP-Glu) was directly measured by MALDI-TOF MS. In nature, one can find unique heme-linked proteins, e.g., cyctochrome *c*. The rHSA(FeP-Glu) conjugate presumably becomes a valuable model of these hemoproteins. The obtained rHSA-(FeP-Glu) can reversibly absorb O_2 under physiological conditions, and its O_2-binding affinity showed an identical value to that for human erythrocytes. These results suggest that this novel plasma protein may efficiently transport O_2 in the bloodstream as an O_2-carrier with a long circulation time.

ACKNOWLEDGMENT

This work was partially supported by Grant-in-Aid for Scientific Research (No. 16350093) from JSPS, Grant-in-Aid for Exploratory Research (No. 16655049) from MEXT Japan, and Health Science Research Grants (Regulatory Science) from MHLW Japan. R.M.W. acknowledges NNSFC (No. 20274034). The authors are grateful to NIPRO Corp. for their supporting the oxygen-infusion project.

Supporting Information Available: Experimental details of the compounds **2**, **3**, **4**, **5**, FeP-Glu, and FeP-GluSu and their spectroscopic data. This material is available free of charge via the Internet at http://pubs.acs.org.

LITERATURE CITED

(1) Peters, T., Jr. (1996) All about albumin. *Biochemistry, Genetics, and Medical Applications*, Academic Press, San Diego; and reference therein.
(2) Kragh-Hansen, U. (1981) Molecular aspects of ligand binding to serum albumin. *Pharmacol. Rev. 33*, 17–53.
(3) Curry, S., Brick, P., and Franks, N. P. (1999) Fatty acid binding to human serum albumin: new insights from crystallographic studies. *Biochim. Biphys. Acta 1441*, 131–140.
(4) (a) Komatsu, T., Hamamatsu, K., Wu, J., and Tsuchida, E. (1999) Physicochemical properties and O_2-coordination structure of human serum albumin incorporating tetrakis(o-pivamido)phenylporphyrinatoiron(II) Derivatives. *Bioconjugate Chem. 10*, 82–86. (b) Tsuchida, E., Komatsu, T., Matsukawa, Y., Hamamatsu, K., and Wu, J. (1999) Human serum albumin incorporating tetrakis(*o*-pivalamido)phenylporphinatoiron(II) derivative as a totally synthetic O_2-carrying hemoprotein. *Bioconjugate Chem. 10*, 797–802. (c) Komatsu, T., Matsukawa, Y., and Tsuchida, E. (2000) Kinetics of CO- and O_2-binding to human serum albumin-heme hybrid. *Bioconjugate Chem. 11*, 772–776. (d) Komatsu, T., Matsukawa, Y., and Tsuchida, E. (2002) Effect of heme structure on O_2-binding properties of human serum albumin-heme hybrids: intramolecular histidine coordination provides a stable O_2-adduct complex. *Bioconjugate Chem. 13*, 397–402. (e) Tsuchida, E., Komatsu, T., Hamamatsu, K., Matsukawa, Y., Tajima, A., Yoshizu, A., Izumi, Y., and Kobayashi, K. (2000) Exchange transfusion of albumin-heme as an artificial O_2-infusion into anesthetized rats: physiological responses, O_2-delivery and reduction of the oxidized hemin sites by red blood cells. *Bioconjugate Chem. 11*, 46–50. (f) Kobayashi, K., Komatsu, T., Iwamaru, A., Matsukawa, Y., Watanabe, M., Horinouchi, H., and Tsuchida, E. (2003) Oxygenation of hypoxia region in solid tumor by administration of human serum albumin incorporating synthetic hemes. *J. Biomed. Mater. Res. 64A*, 48–51. (g) Tsuchida, E., Komatsu, T., Matsukawa, Y., Nakagawa, A., Sakai, H., Kobayashi, K., and Suematsu, M. (2003) Human serum albumin incorporating synthetic heme: red blood cell substitute

without hypertension by nitric oxide scavenging. *J. Biomed. Mater. Res. 64A*, 257–261.

(5) Russo, S. M., Pepe, J. Y., Donohue, S., Cable E. E., Lambrecht, R. W., and Bonkovsky, H. L. (1995) Tissue distribution of zinc-mesoporphyrin in rats: relationship to inhibition of heme oxygenase. *J. Pharmacol. Exp. Ther. 272*, 766–774.

(6) Tsuchida, E., Komatsu, T., Ando, K., Kumamoto, S., and Nishide, H (1995) Synthesis and O_2-binding properties of tetraphenylporphyrinatoiron(II) derivatives bearing a proximal imidazole covalently bound at the β-pyrrolic position. *J. Chem. Soc., Perkin Trans. 2* 1995, 747–753.

(7) The synthetic details and spectroscopic data of the porphyrins can be obtained from the Supporting Information.

(8) Tsuchida, E., Komatsu, T., Arai, K., and Nishide, H. (1993) Synthesis and dioxygen-binding properties of double-sided porphyrinatoiron(II) complexes bearing covalently bound axial imidazole. *J. Chem. Soc., Dalton Trans.* 2465–2469.

(9) (a) Collman, J. P., Brauman, J. I., Collins, T. J., Iverson, B. L., Lang, G., Pettman, R. B., Sessler, J. L., and Walters, M. A. (1983) Synthesis and characterization of the "Pocket" porphyrins. *J. Am. Chem. Soc. 105*, 3038–3052. (b) Collman, J. P., Brauman, J. I., Iverson, B. L., Sessler, J. L., Morris, R. M., and Gibson, Q. H. (1983) O_2 and CO binding to iron(II) porphyrins: a comparison of the "Picket Fence" and "Pocket" porphyrins. *J. Am. Chem. Soc. 105*, 3052–3064.

(10) Tsuchida, E., Komatsu, T., and Yanagimoto, T. (2000) Molecular environment effect on O_2-binding to lipidporphyrinatoiron(II) complexes in aqueous media, *J. Porphyr. 4*, 81–87.

(11) The esff force field simulation was performed using an Insight II system (Molecular Simulations Inc.). The structure was generated by alternative minimizations and annealing dynamic calculations from 1,000 K to 100 K.

(12) Severinghaus, J. W. (1966) Blood gas calculator. *J. Appl. Physiol. 21*, 1108–1116.

(13) Sawicki, C. A., and Gibson G. H. (1977) Properties of the T State of Human Oxyhemoglobin Studied by Laser Photolysis. *J. Biol. Chem. 252*, 7538–7547.

(14) Sharma, V. S., Schmidt, M. R., and Ranney, H. M. (1976) Dissociation of CO from Carboxyhemoglobin. *J. Biol. Chem. 251*, 4267–4272.

(15) Steinmeier, R. C., and Parkhurst, L. J. (1975) Kinetic Studies on the Five Principle Components of Normal Adult Human Hemoglobin. *Biochemistry 14*, 1564–1573.

BC049859M

J|A|C|S
ARTICLES
Published on Web 10/20/2005

O_2 and CO Binding Properties of Artificial Hemoproteins Formed by Complexing Iron Protoporphyrin IX with Human Serum Albumin Mutants

Teruyuki Komatsu,*,† Naomi Ohmichi,† Akito Nakagawa,† Patricia A. Zunszain,‡ Stephen Curry,‡ and Eishun Tsuchida*,†

Contribution from the Advanced Research Institute for Science and Engineering, Waseda University, 3-4-1 Okubo, Shinjuku-ku, Tokyo 169-8555, Japan, and Division of Cell and Molecular Biology, Faculty of Life Sciences, Imperial College London, Huxley Building, South Kensington Campus, London SW7 2AZ, United Kingdom

Received July 18, 2005; E-mail: teruyuki@waseda.jp; eishun@waseda.jp

Abstract: The binding properties of O_2 and CO to recombinant human serum albumin (rHSA) mutants with a prosthetic heme group have been physicochemically and kinetically characterized. Iron(III) protoporphyrin IX (hemin) is bound in subdomain IB of wild-type rHSA [rHSA(wt)] with weak axial coordination by Tyr-161. The reduced ferrous rHSA(wt)−heme under an Ar atmosphere exists in an unusual mixture of four- and five-coordinate complexes and is immediately autoxidized by O_2. To confer O_2 binding capability on this naturally occurring hemoprotein, a proximal histidine was introduced into position Ile-142 or Leu-185 by site-directed mutagenesis. A single mutant (I142H) and three double mutants (I142H/Y161L, I142H/Y161F, and Y161L/L185H) were prepared. Both rHSA(I142H/Y161L)−heme and rHSA(I142H/Y161F)−heme formed ferrous five-*N*-coordinate high-spin complexes with axial ligation of His-142 under an Ar atmosphere. These artificial hemoproteins bind O_2 at room temperature. Mutation at the other side of the porphyrin, Y161L/L185H, also allowed O_2 binding to the heme. In contrast, the single mutant rHSA(I142H)−heme could not bind O_2, suggesting that removal of Y161 is necessary to confer reversible O_2 binding. Laser flash photolysis experiments showed that the kinetics of CO recombination with the rHSA(mutant)−heme were biphasic, whereas O_2 rebinding exhibited monophasic kinetics. This could be due to the two different geometries of the axial imidazole coordination arising from the two orientations of the porphyrin plane in the heme pocket. The O_2 binding affinities of the rHSA(mutant)−heme were significantly lower than those of hemoglobin and myoglobin, principally due to the high O_2 dissociation rates. Changing Leu-161 to Phe-161 at the distal side increased the association rates of both O_2 and CO, which resulted in enhanced binding affinity.

Introduction

Human serum albumin (HSA) is a versatile protein found at high concentrations (4−5 g/dL) in blood plasma and is principally characterized by its remarkable ability to bind a wide range of insoluble endogenous and exogenous compounds.[1] Physiological ligands for HSA include nonesterified fatty acids, hemin, bilirubin, bile acids, and thyroxine,[2−4] but the protein also binds a huge variety of drugs. Currently, it is of great interest to exploit the carrier properties of this shuttle protein for the development of novel therapeutic reagents for drug delivery and pharmacodynamic modulation.[5−7] Hemin [iron(III) protoporphyrin IX] released from hemoglobin (Hb) during the enucleation of red cells or through hemolysis is captured by HSA, which has a high binding constant for this ligand ($K \approx 10^8\ M^{-1}$).[8] This strong affinity of HSA for hemin has stimulated efforts to develop albumin as an artificial hemoprotein which can mimic the O_2 binding capability of Hb and myoglobin (Mb).[9,10] HSA consists of a helical monomer of 66.5 kDa containing three homologous domains (I−III), each of which

† Waseda University.
‡ Imperial College London.

(1) Peters, T. *All about Albumin: Biochemistry, Genetics and Medical Applications*; Academic Press: San Diego, 1996; and references therein.
(2) (a) Kragh-Hansen, U. *Pharmacol. Rev.* **1981**, *33*, 17−53. (b) Kragh-Hansen, U. *Danish Med. Bull.* **1990**, *37*, 57−84.
(3) (a) Curry, S.; Madelkow, H.; Brick, P.; Franks, N. *Nat. Struct. Biol.* **1998**, *5*, 827−835. (b) Bhattacharya, A. A.; Grune, T.; Curry, S. *J. Mol. Biol.* **2000**, *303*, 721−732. (c) Curry, S. Plasma Albumin as a Fatty Acid Carrier. In *Adv. Mol. Cell. Biol.*; van der Vusse, G., Ed.; Elsevier: 2003; Vol. 33, pp 29−46. (d) Petitpas, I.; Petersen, C. E.; Ha, C.-E.; Bhattacharya, A. A.; Zunszain, P. A.; Ghuman, J.; Bhagavan, N. V.; Curry, S. *Proc. Natl. Acad. Sci. U.S.A.* **2003**, *100*, 6440−6445. (e) Zunszain, P. A.; Ghuman, J.; Komatsu, T.; Tsuchida, E.; Curry, S. *BMC Struct. Biol.* **2003**, *3*, 6.
(4) (a) He, X. M.; Carter, D. C. *Nature* **1992**, *358*, 209−215. (b) Carter, D. C.; Ho, J. X. *Adv. Protein Chem.* **1994**, *45*, 153−203. (c) Wardell, M.; Wang, Z.; Ho, J. X.; Robert, J.; Ruker, F.; Rubel, J.; Carter, D. C. *Biochem. Biophys. Res. Commun.* **2002**, *291*, 813−819.
(5) Beljaars, L.; Molema, G.; Schuppan, D.; Geerts, A.; De Bleser, P. J.; Weert, B.; Meijer, D. K. F.; Poelstra, K. *J. Biol. Chem.* **2000**, *275*, 12743−12751.
(6) Kurtzhals, P.; Havelund, S.; Jonassen, I.; Kiehr, B.; Larsen, U. D.; Ribel, U.; Markussen, J. *Biochem. J.* **1995**, *312*, 725−731.
(7) Sheffield, W. P. *Curr. Drug Targets Cardiovasc. Haematol. Disord.* **2001**, *1*, 1−22.
(8) Adams, P. A.; Berman, M. C. *Biochem. J.* **1980**, *191*, 95−102.
(9) (a) Komatsu, T.; Hamamatsu, K.; Wu, J.; Tsuchida, E. *Bioconjugate Chem.* **1999**, *10*, 82−86. (b) Tsuchida, E.; Komatsu, T.; Matsukawa, Y.; Hamamatsu, K.; Wu, J. *Bioconjugate Chem.* **1999**, *10*, 797−802. (c) Komatsu, T.; Matsukawa, Y.; Tsuchida, E. *Bioconjugate Chem.* **2002**, *13*, 397−402.

10.1021/ja054819u CCC: $30.25

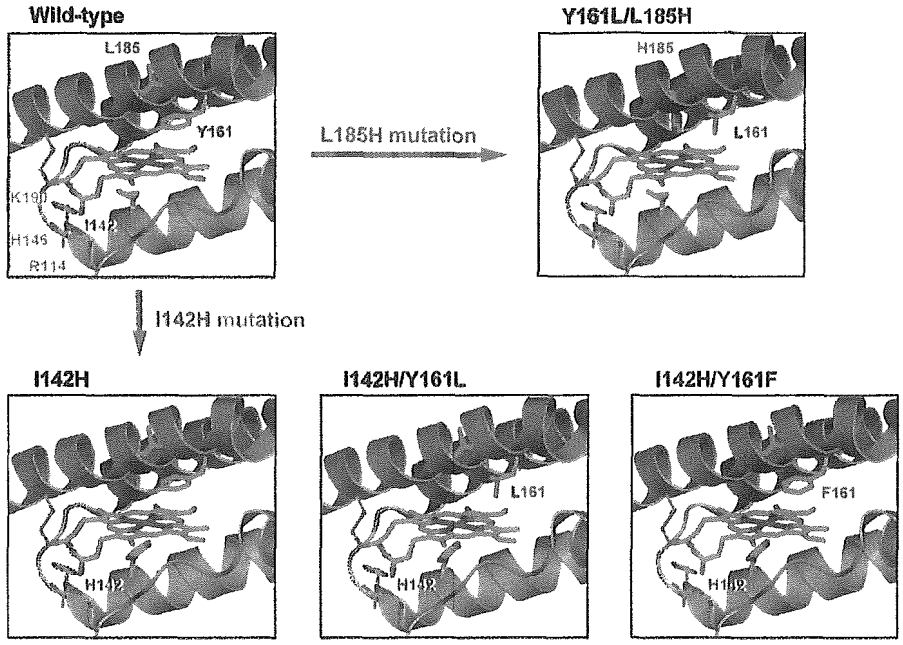

Figure 1. Structural models of the effect of site-directed mutagenesis in subdomain IB of HSA to construct a tailor-made heme pocket, which allows O_2 binding to the prosthetic Fe^{2+} protoporphyrin IX (heme) group.[12]

is composed of A and B subdomains. Crystallographic studies have revealed that hemin is bound within a narrow D-shaped hydrophobic cavity in subdomain IB with axial coordination of Tyr-161 to the central ferric ion and electrostatic interactions between the porphyrin propionates and a triad of basic amino acid residues (Arg-114, His-146, and Lys-190) (Figure 1).[3e,4c] In terms of the general hydrophobicity of this α-helical heme pocket, the subdomain IB of HSA potentially has similar features to the heme binding site of Hb or Mb. However, if one reduces the HSA–hemin to obtain the ferrous complex, it is rapidly oxidized by O_2 even at low temperature (~0 °C). This is due to the fact that HSA lacks the proximal histidine which in Hb and Mb enables the prosthetic heme group to bind O_2 and serves to regulate the O_2 binding affinity.

On the basis of the crystal structure of the HSA–hemin complex, we have used site-directed mutagenesis to introduce into the heme binding site of HSA a histidine that would be predicted to provide axial coordination to the central Fe^{2+} atom of the heme and thereby promote O_2 binding (Figure 1). An initial recombinant HSA mutant, in which Ile-142 and Tyr-161 were replaced by His and Leu, respectively [rHSA(I142H/Y161L)], has been made, and the O_2 binding capabilities of the heme complex have been partially evaluated.[11] In the present study, we have elucidated the coordination structure of the naturally occurring wild-type rHSA–heme [rHSA(wt)–heme] by UV–vis and magnetic circular dichroism (MCD) spectroscopies and characterized the unusual axial coordination of Tyr-161 to the heme. To develop HSA–heme as a synthetic O_2 carrier, we have also generated several new mutant rHSA–heme complexes. Their O_2 and CO binding properties have been characterized kinetically and compared to those of the natural Hb, Mb, and recombinant Mb (rMb) mutants. We have shown that our mutagenesis approach can create a new class of albumin-based artificial hemoproteins which would serve as an O_2 carrier.

Experimental Section

Materials and Apparatus. rHSA(wt) was kindly provided by the NIPRO Corp. (Osaka, Japan). All reagents were purchased from commercial sources as special grades and used without further purification unless otherwise noted. Iron(III) protoporphyrin IX (hemin) chloride was purchased from Fluka. Horse skeletal muscle myoglobin (Mb) was purchased from Sigma-Aldrich. The iron(III) protoporphyrin IX dimethyl ester chloride (FePPIXDME) was prepared by esterification of carboxylate side chains of hemin with acidic methanol. The UV–vis absorption spectra were recorded using an Agilent 8453 UV–visible spectrophotometer fitted with an Agilent 89090A temperature control unit.

Site-Directed Mutagenesis, Protein Expression, and Purification. Specific mutations were introduced into HSA within the context of a plasmid vector containing the entire HSA coding region (pHIL-D2 HSA) using designed primers with the QuikChange XL site-directed mutagenesis kit (Stratagene).[13] All mutations were confirmed by DNA sequencing. Each mutated pHIL-D2 HSA plasmid was linearized by NotI digestion and introduced into *Pichia pastoris GS115* by electroporation using a BioRad MicroPulser. Expressions were carried out by standard protocols (Invitrogen) with some modifications. Clones were grown upon BMGY medium [1% yeast extract, 2% peptone, 0.1 M potassium phosphate (pH 6.0), 1.34% yeast nitrogen base without amino acids, 40 ppm biotin, 1% glycerol] and transferred to BMMY medium [1% yeast extract, 2% peptone, 0.1 M potassium phosphate (pH 6.0), 1.34% yeast nitrogen base without amino acids, 40 ppm biotin, 1% methanol] for induction with methanol in baffled shaking flasks at 30 °C in a JEIOTECH SI-600R incubator at 200 rpm.

(10) Marden, M. C.; Hazard, E. S.; Leclerc, L.; Gibson, Q. H. *Biochemistry* **1989**, *28*, 4422–4426.
(11) Komatsu, T.; Ohmichi, N.; Zunszain, P. A.; Curry, S.; Tsuchida, E. *J. Am. Chem. Soc.* **2004**, *126*, 14304–14305.
(12) The pictures were produced on the basis of crystal structure coordinate of the rHSA(wt)-hemin (code: 1O9X, ref 3e) using PyMOL. DeLano, W. L. The PyMOL Molecular Graphics System 2002 DeLano Scientific, San Carlos, CA.
(13) (a) Peterson, C. E.; Ha, C.-E.; Jameson, D. M.; Bhagavan, N. V. *J. Biol. Chem.* **1996**, *271*, 19110–19117. (b) Peterson, C. E.; Ha, C.-E.; Harohalli, K.; Park, D.; Bhagavan, N. V. *Biochemistry* **1997**, *36*, 7012–7017.

The secreted rHSA was isolated as follows. The growth medium was centrifuged to harvest the culture supernatant, which was brought to 50% saturation by the addition of solid ammonium sulfate with stirring at room temperature. The mixture was then incubated at 4 °C for 1 h. The resulting precipitate was removed by centrifugation, and the supernatant fluid was brought to 95% saturation with ammonium sulfate. The precipitated protein, which contains rHSA, was collected by centrifugation and dissolved in distilled water. The brownish solution was dialyzed for 48 h at 4 °C against 100 volumes of distilled water, followed by 24 h against 100 volumes of 50 mM potassium phosphated buffer (pH 7.0). The dialysate was then loaded onto a Cibacron Blue column of Blue Sepharose 6 Fast Flow (Amersham Pharmacia Biotech) and washed with 10 bed volumes of 50 mM potassium phosphate. Elution of the rHSA(mutant) was carried out with 3 M NaCl and the eluent dialyzed against 50 mM potassium phosphate. After concentration using an ADVANTEC Q0100 ultrafilter (10 kDa Mw cutoff) in an UHP-43K ultraholder, the samples were applied to a Superdex 75 column (Amersham Pharmacia Biotech) using 50 mM potassium phosphate as the running buffer. All the purification steps were followed by SDS–PAGE analysis. Each rHSA(mutant) exhibited a single band and migrated the same distance as rHSA(wt). The protein concentration was assayed by measuring the absorbance at 280 nm ($\epsilon_{280} = 3.4 \times 10^4$ M^{-1} cm^{-1}).

Preparations of rHSA–Hemin and rHSA–Heme Complexes. The ferric rHSA(mutant)–hemin complexes were prepared according to our previously reported procedures for rHSA(wt)–hemin.[3e] Typically 5 mL of 0.1 mM rHSA(mutant) in 50 mM potassium phosphate (pH 7.0) was mixed with 0.8 mL of 0.688 mM hemin in DMSO [hemin:rHSA-(mutant) molar ratio of 1.1] and incubated overnight with rotation in the dark at room temperature. The complex was then diluted with 50 mM potassium phosphate (200 mL) and concentrated to the initial volume (5.8 mL) using an ADVANTEC Q0100 ultrafilter (10 kDa Mw cutoff). These dilution and concentration cycles were repeated to reduce the final concentration of DMSO to <0.1 vol %. The resulting samples were analyzed by a SDS–PAGE to confirm the protein integrity and concentration.

The 50 mM phosphate-buffered solution (pH 7.0) of rHSA(mutant)–hemin ([hemin] = ca. 10 μM) in a 10 mm path length optical quartz cuvette sealed with a rubber septum was purged with Ar for 40 min. A small excess amount of degassed aqueous sodium dithionate was added by microsyringe to the sample under an Ar atmosphere to reduce the central ferric ion of the hemin, generating the deoxy ferrous rHSA-(mutant)–heme complexes.

Kinetic Measurements for O_2 and CO Bindings. Kinetics studies were carried out using laser flash photolysis techniques at 22 °C, except for the determination of the CO dissociation rates. Laser flash photolysis experiments were performed using a Unisoku TSP-1000WK time-resolved spectrophotometer with a Spectron Laser Systems SL803G-10 Q-switched Nd:YAG laser, which generated a second-harmonic (532 nm) pulse of 6 ns duration (10 Hz). The probe light from a 150 W xenon arc-lamp was passed through an UV cutoff filter and an Asahi Spectra MC filter before irradiation to minimize any sample damage. Normally, fresh solutions of the deoxy rHSA(mutant)–heme were made up for each set of experiments, and the gas mixture with the desired partial pressure of O_2/CO/N_2 prepared by a KOFLOC Gasblender GB-3C was flowed into the sample cuvette for 20 min for equilibration.

In general, recombination following laser flash photolysis to hemeO_2 or hemeCO occurs according to eq 1 with the association rate constant (k_{on}^{L}), dissociation rate constant (k_{off}^{L}), and apparent rate constant (k_{app}) given by eq 2.[14,15] The values of k_{app} were obtained directly from the log plots of the change in absorbance (ΔA) versus time. The gas

$$\text{hemeL} \xrightarrow{h\nu} \text{heme} \underset{k_{off}^{L}}{\overset{k_{on}^{L}}{\rightleftharpoons}} \text{hemeL} \quad [\text{L} = \text{O}_2 \text{ or CO}] \tag{1}$$

$$k_{app} = k_{on}^{L}[\text{L}] + k_{off}^{L} \tag{2}$$

concentrations were always higher than that of the heme; therefore, the pseudo-first-order approximation can be applied throughout. For CO rebinding at high [CO], eq 2 reduces to eq 3 because $k_{on}^{CO}[CO] \gg k_{off}^{CO}$.

$$k_{app} \approx k_{on}^{CO}[CO] \tag{3}$$

Thus, k_{on}^{CO} of the rHSA(mutant)–heme was easily calculated from k_{app}/[CO].

The O_2 association rates ($k_{on}^{O_2}$) and the O_2 binding constants [$K^{O_2} = (P_{1/2}^{O_2})^{-1}$] of the rHSA(mutant)–heme were measured using the competitive rebinding technique.[14,15] Photolysis of hemeCO in the presence of CO and O_2 gives the five-*N*-coordinate heme (deoxy state), which is first trapped as hemeO_2 and subsequently converted back to hemeCO (eq 4).

$$\text{hemeCO} \underset{k_{on}^{CO}}{\overset{k_{off}^{CO}}{\rightleftharpoons}} \text{heme} \underset{k_{off}^{O_2}}{\overset{k_{on}^{O_2}}{\rightleftharpoons}} \text{heme}O_2 \tag{4}$$

The CO concentration was held constant, and the fast and slow kinetics were measured at different [O_2]. The fast process is given by eq 5, allowing the direct determination of $k_{on}^{O_2}$ from a plot of k_{app}(fast) versus [O_2].

$$k_{app}(\text{fast}) = k_{on}^{O_2}[O_2] + k_{off}^{O_2} + k_{on}^{CO}[CO] \tag{5}$$

The rate constant for the slower process, k_{app}(slow), is substituted into Traylor's eq 6 to obtain K^{O_2} [$=(P_{1/2}^{O_2})^{-1}$].[15]

$$\frac{k_{on}^{CO}[CO]}{k_{app}(\text{slow})} = K^{O_2}[O_2] + \frac{k_{on}^{CO}[CO]}{k_{off}^{O_2}} + 1 \tag{6}$$

The value of $k_{on}^{CO}[CO]$ is constant; therefore, the plots of $k_{on}^{CO}[CO]/k_{app}$(slow) versus [O_2] affords K^{O_2}.

The relaxation curves that accompanied the O_2 or CO recombination were fitted to single- or double-exponentials using the Unisoku Spectroscopy & Kinetics Software. The $k_{off}^{O_2}$ values can be determined from the *y*-intercept of eq 5 or 6, but they often have large deviations. Therefore, we calculated $k_{off}^{O_2}$ from $k_{on}^{O_2}/K^{O_2}$ (both obtained from slopes).

The CO dissociation from the rHSA(mutant)–hemeCO was measured by carrying out the replacement reaction with NO.[16] A Sephadex G-25 column was equilibrated with CO-saturated potassium phosphate buffer (50 mM, pH 7.0), and the rHSA(mutant)–hemeCO solution was passed through the column to remove the dithionate. The eluent was directly connected to a optical quartz cuvette under a 10% CO (in N_2) atmosphere. The 10% NO (in N_2) equilibrated buffer was then rapidly injected into the rHSA(mutant)–hemeCO solution, and the time dependence of the decrease in absorption at 418 nm was monitored. The relaxation curves that accompanied the CO dissociation within several minutes were analyzed by fitting to double-exponentials. The CO binding constants [$K^{CO} = (P_{1/2}^{CO})^{-1}$] were calculated using k_{on}^{CO}/k_{off}^{CO}.

Magnetic Circular Dichroism (MCD). The MCD for the 50 mM potassium phosphate-buffered solutions (pH 7.0) of the rHSA(wt)–heme and rHSA(mutant)–heme series (8.0 μM) under Ar and CO atmospheres were measured using a JASCO J-820 circular dichrometer fitted with a 1.5 T electromagnet at 22 °C. The spectrum was acquired five times to improve signal-to-noise, and each data point was corrected

(14) Collman, J. P.; Brauman, J. I.; Iverson, B. L.; Sessler, J. L.; Moris, R. M.; Gibson, Q. H. *J. Am. Chem. Soc.* **1983**, *105*, 3052–3064.
(15) Traylor, T. G.; Tsuchiya, S.; Campbell, D.; Mitchel, M.; Stynes, D.; Koga, N. *J. Am. Chem. Soc.* **1985**, *107*, 604–614.
(16) Rohlfs, R.; Mathews, A. J.; Carver, T. E.; Olson, J. S.; Springer, B. A.; Egeberg, K. D.; Sliger, S. G. *J. Biol. Chem.* **1990**, *265*, 3168–3176.

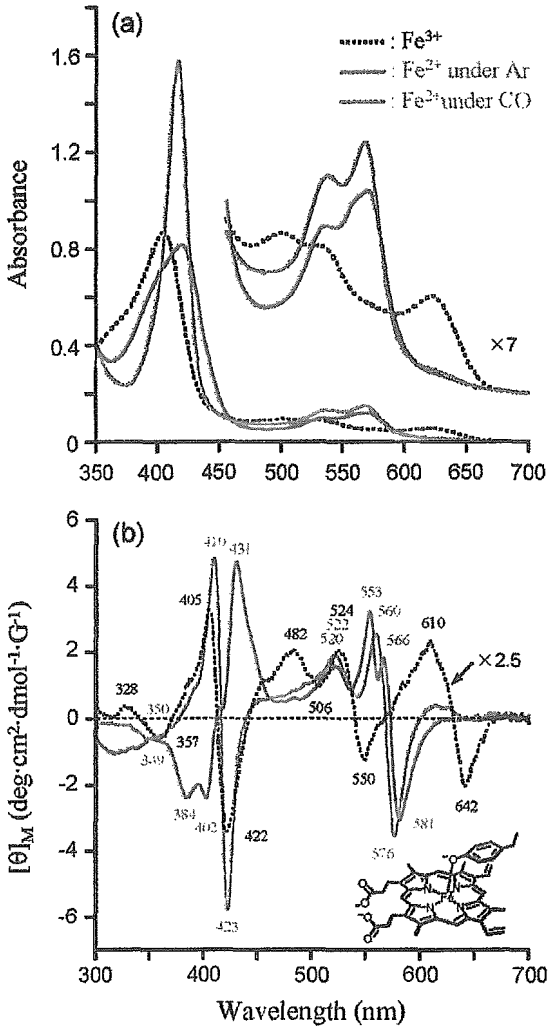

Figure 2. (a) UV−vis absorption and (b) MCD spectral changes of the rHSA(wt)-heme in 50 mM potassium phosphate buffered solution (pH 7.0, 22 °C).

by subtracting the optical rotation observed in the absence of an applied magnetic field.

Results and Discussion

Naturally Occurring rHSA(wt)−Hemin. Our crystal structure analysis revealed that hemin is bound within a D-shaped cavity in subdomain IB of rHSA(wt), where the central ferric ion is coordinated by Tyr-161, and the two propionate side chains are coordinated by a triad of basic amino acid residues (Figure 1).[3e] The UV−vis absorption spectrum of the phosphate-buffered solution (50 mM, pH 7.0) of rHSA(wt)−hemin showed a Soret band at 405 nm and the charge-transfer (CT) band of the porphyrin $p\pi$ to the Fe^{3+} $d\pi$ orbitals at 624 nm (Figure 2a). The spectral pattern and amplitudes were almost constant in the temperature range of 5−40 °C. The dominant feature of the spectrum was quite similar to those of the human or horse heart ferric H93Y recombinant Mb [rMb(H93Y)], in which the proximal histidine (His-93) was replaced with Tyr by site-directed mutagenesis (Table 1).[17,18] Adachi and co-workers showed that the ferric rMb(H93Y) formed a five-coordinate high-spin complex with a single oxygen donor of the proximal

Table 1. UV-vis Absorption Spectral Data of the rHSA(wt)-Heme, rHSA(mutant)-Heme and Other Hemoproteins

Hemoproteins	State	λ_{max} (nm) Soret	Visible
rHSA(wt)-Heme[a]	Fe^{3+}	405	501, 534, 624
	Fe^{2+}	419	538, 559(sh), 570
	$Fe^{2+}CO$	416	539, 568
HSA-Heme[b]	Fe^{3+}	404	498, 530, 620
	Fe^{2+}	416	534, 570
	$Fe^{2+}CO$	418	536, 568
Human rMb(H93Y)[c]	Fe^{3+}	402	480, 520(sh), 598
	Fe^{2+}	427	560
	$Fe^{2+}CO$	420	539, 567
Horse Heart rMb(H93Y)[d]	Fe^{3+}	403	487, 524, 599
	Fe^{2+}	429	556
	$Fe^{2+}CO$	419	539, 570
FePPIXDME(CH_3O^-)[e]	Fe^{3+}	401	476, 580(sh), 600
FePPIXDME(p-NO_2PhO^-)[f]	Fe^{3+}	402	500, 528, 621
FePPIXDME[a,g]	Fe^{3+}	400	571, 599
	Fe^{2+}	393, 414, 427, 440(sh)	535, 571
	$Fe^{2+}CO$	411	532, 564
rHSA(I142H)-Heme[a]	Fe^{3+}	404	501, 533, 619
	Fe^{2+}	424	530, 558
	$Fe^{2+}CO$	419	537, 560
rHSA(I142H/Y161L)-Heme[a]	Fe^{3+}	402	533, 620
	Fe^{2+}	426	531(sh), 559
	$Fe^{2+}O_2$	412	537, 573
	$Fe^{2+}CO$	419	538, 565
rHSA(I142H/Y161Y)-Heme[a]	Fe^{3+}	402	533, 620
	Fe^{2+}	425	532(sh), 559
	$Fe^{2+}O_2$	411	538, 576
	$Fe^{2+}CO$	419	538, 565
rHSA(Y161L/L185H)-Heme[a]	Fe^{3+}	408	528, 620
	Fe^{2+}	422	530, 558
	$Fe^{2+}O_2$	412	538, 570
	$Fe^{2+}CO$	419	537, 560
Mb[a,h]	Fe^{3+}	409	503, 548(sh), 632
	Fe^{2+}	434	557
	$Fe^{2+}O_2$	418	544, 581
	$Fe^{2+}CO$	423	541, 579

[a] In 50 mM potassium phosphate buffer (pH 7.0, 22 °C). [b] In 0.1 M phosphate buffer (pH 7.0); ref 22. [c] In 50 mM sodium phosphate buffer (pH 7.0, 20 °C); ref 17. [d] At pH 7−10, 25 °C; ref 18. [e] In CH_2Cl_2/CH_3OH = 9/1 (v/v) (25 °C); ref 21. [f] In CH_2Cl_2 (25 °C); ref 21. [g] In 0.5% Me_3CeNBr. [h] Horse muscle Mb (Sigma).

Tyr-93 by resonance Raman spectroscopy.[17b] Our absorption spectral data imply that the hemin is bound to Tyr-161 of rHSA-(wt) and forms a ferric five-coordinate high-spin complex under physiological conditions. Interestingly, the CT absorptions of the rHSA(wt)−hemin appeared at a higher wavelength (λ_{max} = 624 nm) compared to rMb(H93Y) (λ_{max} = 598−599 nm). Dawson and co-workers classified the CT bands of the oxygen-ligated hemins into two groups: the first at around 600 nm for rMb(H93Y) and the methoxide (CH_3O^-) complex of Fe^{3+} protoporphyrin IX dimethyl ester (Fe^{3+}PPIXDME), and the second at around 620 nm for p-nitrophenolate (p-NO_2PhO^-) or the acetate complex of Fe^{3+}PPIXDME, in which the nonoccupied π^* orbitals of the fifth ligand interacts with the Fe^{3+} $d\pi$ orbitals and, in turn, lowered the energy level of the CT transition (Table 1).[19] The rHSA(wt)−hemin definitely belongs to the latter group, which suggests that the axial coordination

(17) (a) Adachi, S.; Nagano, S.; Watanabe, Y.; Ishimori, K.; Morishima, I. *Biochim. Biophys. Res. Commun.* **1991**, *180*, 138−144. (b) Adachi, S.; Nagano, S.; Ishimori, K.; Watanabe, Y.; Morishima, I.; Egawa, T.; Kitagawa, T.; Makino, R. *Biochemistry* **1993**, *32*, 241−252.
(18) Hildebrand, D. P.; Burk, D. L.; Maurus, R.; Ferrer, J. C.; Brayer G. D.; Mauk, A. G. *Biochemistry* **1995**, *34*, 1997−2005.
(19) Pond, A. E.; Roach, M. P.; Sono, M.; Rux, A. H.; Franzen, S.; Hu, R.; Thomas, M. R.; Wilks, A.; Dou, Y.; Ikeda-Saito, M.; Oritz de Montellano, P. R.; Woodruff, W. H.; Boxer, S. G.; Dawson, J. H. *Biochemistry* **1999**, *38*, 7601−7608.

of Tyr-161 to the hemin is weaker than that of rMb(H93Y) and Fe^{3+}PPIXDME(CH_3O^-). This is consistent with the observation that the Fe^{3+}−O(phenolate) distance in the crystal structure of the rHSA(wt)−hemin (2.78 Å) is greater than that for rMb-(H93Y) (1.91 Å).[3e]

We then employed MCD spectroscopy to elucidate the axial coordination environment of the rHSA(wt)−hemin. MCD is a powerful probe of the oxidation state, spin state, and the nature of the axial ligand in heme system and has frequently been used as a method of comparison between synthetic iron porphyrins of known axial ligation and newly discovered hemoproteins of unknown ligation.[20] The ferric rHSA(wt)−hemin showed a characteristic MCD pattern with two distinct troughs in the visible region (550, 642 nm) (Figure 2b), which was more similar to that of the five-coordinate Fe^{3+}PPIXDME (p-NO_2-PhO^-) than to that of the Fe^{3+}PPIXDME(CH_3O^-).[19,21] The MCD of the rHSA(wt)−hemin therefore also supports the formation of a five-coordinate high-spin hemin complex with weak axial ligation by Tyr-161.

Reduced Ferrous rHSA(wt)−Heme. Reduction of the ferric rHSA(wt)−hemin by the addition of sodium dithionate under an Ar atmosphere gave a ferrous heme complex with a broad Soret band at 419 nm ($\Delta\lambda_{1/2}$ = 61 nm) and two definite Q-bands at 538 and 570 nm (Figure 2a). This is in significant contrast to human ferrous rMb(H93Y) in a five-coordinate high-spin complex, which exhibits a similar spectrum to deoxy Mb with a sharp Soret band and single Q-band absorption around 560 nm (Table 1).[17,18] The shoulder at 559 nm in the spectrum of the rHSA(wt)−heme is probably due to a ferrous five-coordinate complex, but this clearly coexists with another species. One possible candidate is a six-coordinate low-spin complex. Casella and co-workers proposed that the reduced HSA−heme contains a six-coordinate heme.[22] Nevertheless, the MCD spectrum of the ferrous rHSA(wt)−heme (Figure 2b) was quite different from the well-known shape of the six-coordinate low-spin heme derivatives, such as cytochrome b_5 and bisimidazole-ligated Fe^{2+} PPIXDME, which show a sharp and intense Faraday A term corresponding to the α band.[20c]

Another possibility is a four-coordinate intermediate spin state (S = 1) not found in natural Mb. Phosphate-buffered solutions (pH 7.0) of 0.5% (w/v) N-cetyltrimethylammonium bromide ($CetMe_3NBr$) micelles containing dissolved Fe^{2+}PPIXDME showed a multiple broad Soret band ($\Delta\lambda_{1/2}$ = 73 nm) and well-defined β and α bands (535 and 571 nm) (Table 1, see Figure S1a), a spectral pattern consistent with a four-coordinate Fe^{2+}-mesoporphyrin IX dimethyl ester in the $CetMe_3NBr$ suspension.[23] This observation suggests that the strong β and α bands (538, 570 nm) in the UV−vis absorption spectrum of the rHSA-(wt)−heme complex also derived from a ferrous four-coordinate complex. The micellar solution of Fe^{2+}PPIXDME showed complicated MCD bands in the Soret region and two positive peaks (522, 562 nm) and one trough (579 nm) in the visible region (see Figure S1b). The typical MCD of five-coordinate deoxy Mb is shown in Figure 4b (vide infra). Comparison of these data with the MCD spectral pattern of ferrous rHSA(wt)−heme suggests that the latter involves both important features of four- and five-coordinate heme complexes (Figure 2b). Therefore, we conclude that the reduced ferrous rHSA(wt)−heme is in an unusual mixture of a five-coordinate high-spin complex (S = 5/2) with Tyr-161 and a four-coordinate intermediate spin state (S = 1) under an Ar atmosphere. The estimated ratio of the five- and four-coordinate complexes is approximately 1/1.

Upon the addition of O_2 gas to this solution, the central ferrous ion was rapidly autoxidized even at low temperature (~0 °C), and the UV−vis absorption spectrum returned to the initial ferric complex. On the other hand, a carbonyl complex was formed at room temperature and exhibited a very similar absorption (λ_{max} = 416, 539, 568 nm) to human and horse rMb-(H93Y)CO (Figure 2a, Table 1).[17,18] The MCD spectrum of the rHSA(wt)−hemeCO showed simple Faraday A terms associated with the porphyrin $\pi-\pi^*$ transitions, which are typical of a low-spin carbonyl heme (Figure 2b).[20] The rHSA(wt)−hemeCO could be a diamagnetic low-spin complex with a phenolate ligand (Tyr-161) similar to what was found for rMb(H93Y).

In our blood stream, the most avid carrier of hemin is the specific heme-binding protein, hemopexin.[24,25] The binding constant of hemopexin for hemin is 10^4-fold higher than HSA. However, due to the extremely low abundance of hemopexin in plasma (<17 μM), HSA acts as a significant depot of hemin in the circulation. The hemin binding to these proteins not only conserves the porphyrin iron and channels it to the specific catabolism site but it also prevents its toxic effects, such as the catalysis of hydroxyl radical production. Furthermore, HSA−hemin exhibits little peroxidase or catalase activities.[22] The weak axial coordination of phenolate to HSA-bound hemin may therefore have evolved for (1) easy release and transfer to hemopexin in the blood stream, and (2) maintenance of the antioxidative homeostasis in the extracellular fluids of our body.

Genetic Engineered rHSA(mutant) Complexed with Hemin. The detailed architecture of the heme-binding site in HSA revealed by our crystallographic studies allows us to design mutagenesis experiments to construct a tailor-made heme pocket for stable O_2 binding. Tyr-161 was the first candidate considered for site-directed mutagenesis to introduce a proximal histidine; however, the Y161H mutation was not done because our simulations indicated that the distance from N_ϵ(H161) to Fe-(heme) would be too great (4.0 Å). Instead, modeling experiments suggested that the favorable positions for the axial imidazole insertion would be Ile-142 and Leu-185 (Figure 1). The N_ϵ(histidine)−Fe distances were estimated to be 2.31 Å for H142 and 2.69 Å for H185 (compared to 2.18 Å for Mb). We therefore designed and produced a single mutant I142H and three double mutants I142H/Y161L, I142H/Y161F, and Y161L/L185H (see Experimental Section).

The UV−vis absorption and MCD spectra of the rHSA-(I142H/Y161L)−hemin and rHSA(I142H/Y161F)−hemin are

(20) (a) Collman, J. P.; Basolo, F.; Bunnenberg, E.; Collins, T. J.; Dawson, J. H.; Ellis, P. E., Jr.; Marrocco, M. L.; Moscowitz, A.; Sessler, J. L.; Szymanski, T. *J. Am. Chem. Soc.* **1981**, *103*, 5636−5648. (b) Cheek, J.; Dawson, J. H. Magnetic Circular Dichroism Spectroscopy of Heme Proteins and Model Systems. In *The Porphyrin Handbook*; Kadish, K. M., Smith, K. M., Guilard, R., Eds.; Academic Press: San Diego, 2000; Vol. 7, pp 339−369. (c) Svastits, E. W.; Dawson, J. H. *Inorg. Chim. Acta.* **1986**, *123*, 83−86.

(21) Nozawa, T.; Okubo, S.; Hatano, M. *J. Inorg. Biochem.* **1980**, *12*, 253−267.

(22) Monzani, E.; Bonafè, B.; Fallarini, A.; Redaelli, C.; Casella, L.; Minchiotti, L.; Galliano, M. *Biochim. Biophys. Acta* **2001**, *1547*, 302−312.

(23) Geibel, J.; Cannon, J.; Campbell, D.; Traylor, T. G. *J. Am. Chem. Soc.* **1978**, *100*, 3575−3585.

(24) Tolosano, E.; Altruda, F. *DNA Cell Biol.* **2002**, *21*, 297−306.

(25) Paoli, M.; Anderson, B. F.; Baker H. M.; Morgan, W. T.; Smith, A.; Baker, E. N. *Nat. Struct. Biol.* **1999**, *6*, 926−931.

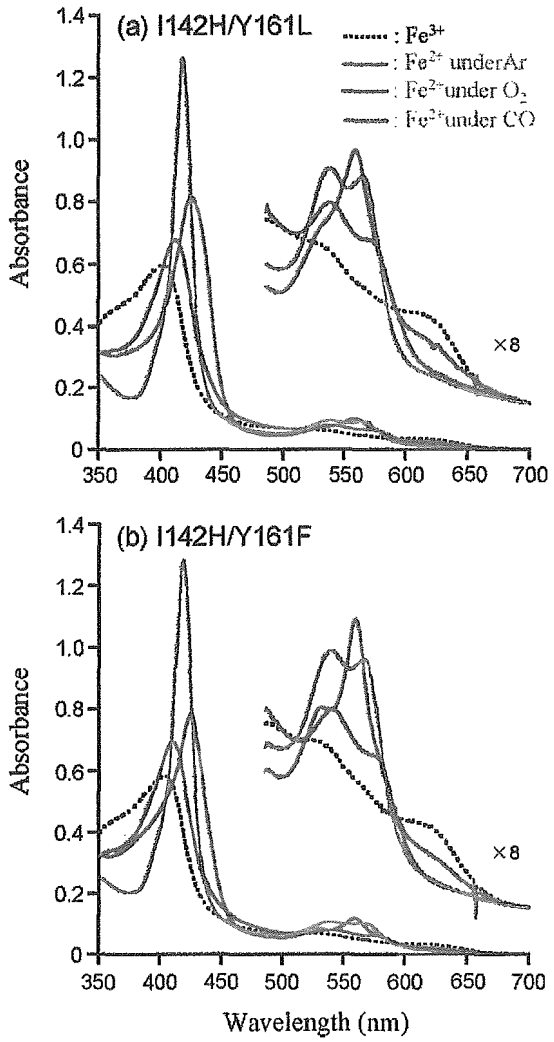

Figure 3. UV-vis absorption spectral changes of the (a) rHSA(I142H/Y161L)-heme and (b) rHSA(I142H/Y161F)-heme in 50 mM potassium phosphate buffered solution (pH 7.0, 8 °C).

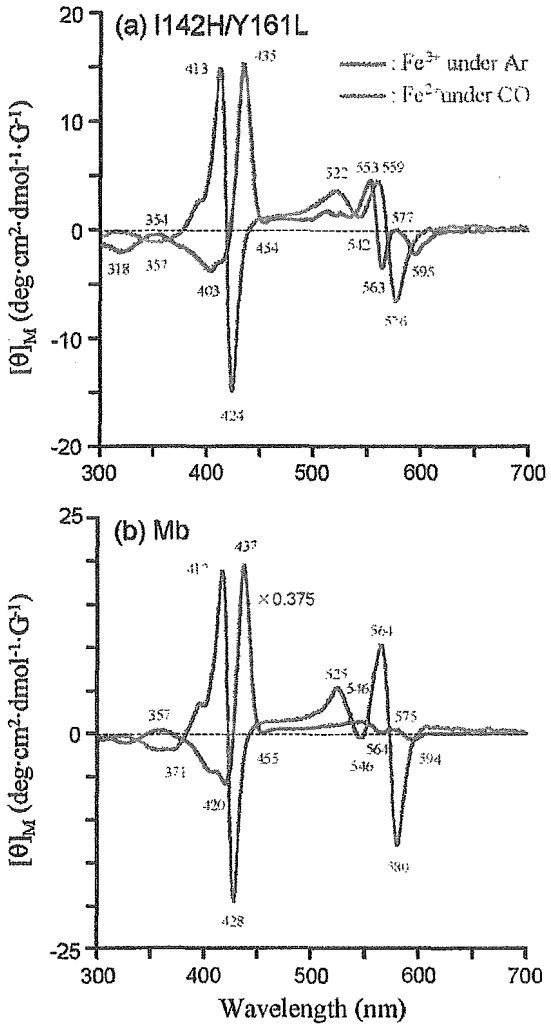

Figure 4. MCD spectral changes of the (a) rHSA(I142H/Y161L)-heme and (b) native Mb in 50 mM potassium phosphate buffered solution (pH 7.0, 22 °C).[30]

essentially the same in their general features (Figure 3 and Figure S2). The strong absorption band due to the porphyrin-to-metal CT was weakened because of the Y161L and Y161F mutations (Figure 3). Both MCD spectra showed similar S-shaped patterns in the Soret band region, which resembled that of ferric Mb (see Figure S2).[26] It is known that two water molecules are located in the heme pocket of ferric Mb.[27] One water axially coordinates to the sixth position of the central ferric ion of the hemin to produce the aquo complex, and the other one is at the rear of the pocket, hydrogen bonded to the first water. A great number of MCD studies on synthetic iron porphyrins and hemoproteins have demonstrated that the spectral shape in the Soret region can be used as a qualitative marker of the spin state and axial coordination environment.[20] Vickery and co-workers found that (i) the Soret MCD intensity of the ferric Mb with different anions at the six-coordinate position was correlated with the amount of low-spin component formed, and (ii) the shape of the band is sensitive to the nature of the sixth ligand.[26] Our MCD results suggest that both the rHSA-(I142H/Y161L)−hemin and rHSA(I142H/Y161F)−hemin are in predominantly ferric high-spin complexes having a water molecule as the sixth ligand.

O_2 and CO Binding to Ferrous rHSA(mutant)−Heme. The rHSA(mutant)−hemin was easily reduced to the ferrous complex by adding a small molar excess of aqueous sodium dithionate under an Ar atmosphere. A single broad absorption band (λ_{max} = 559 nm) in the visible region of the rHSA(I142H/Y161L)−heme and rHSA(I142H/Y161F)−heme was similar to that observed for deoxy Mb[28] or the chelated heme in DMF,[29] indicating the formation of a five-*N*-coordinate high-spin complex (Figure 3, Table 1). The spectral features and amplitude were unaltered in the temperature range of 0−25 °C. The heme therefore appears to be accommodated in the mutated heme pocket with an axial coordination involving His-142. Upon exposure of the rHSA(I142H/Y161L)−heme and rHSA(I142H/

(26) Vickery, L.; Nozawa, T.; Sauer, K. *J. Am. Chem. Soc.* **1976**, *98*, 343−350.
(27) Springer, B. A.; Sligar, S. G.; Olson, J. S.; Phillips, G. N., Jr. *Chem. Rev.* **1994**, *94*, 699−714.
(28) Antonini, E.; Brunori, M. *Hemoglobin and Myoglobin in Their Reactions with Ligands*; North-Holland Pub.: Amsterdam, 1971; p 18.
(29) Traylor, T. G.; Chang, C. K.; Geibel, J.; Berzinis, A.; Mincey, T.; Cannon, J. *J. Am. Chem. Soc.* **1979**, *101*, 6716−6731.